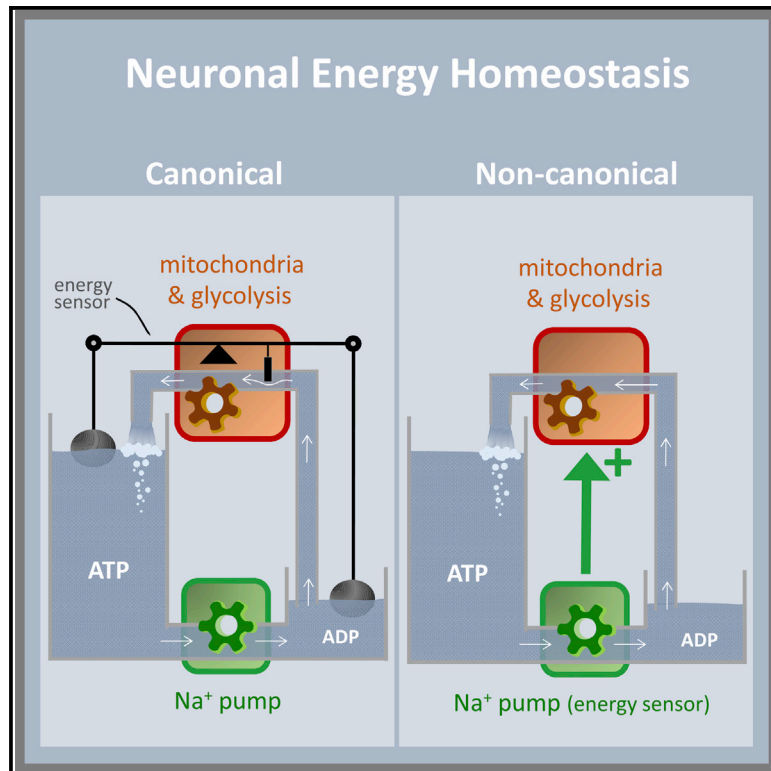


Cell Metabolism

Non-Canonical Control of Neuronal Energy Status by the Na⁺ Pump

Graphical Abstract



Authors

Felipe Baeza-Lehnert, Aiman S. Saab, Robin Gutiérrez, ..., Johannes Hirrlinger, Bruno Weber, L. Felipe Barros

Correspondence

fbarros@cecs.cl

In Brief

Using fluorescent sensors for ions and metabolites Baeza-Lehnert et al. mapped the metabolic response to synaptic transmission *in vitro* and *in vivo*. Neurons showed perfect energetic stability that was attributed to control of ATP production by the Na⁺ pump, as opposed to conventional homeostasis mediated by ADP, ATP, and Ca²⁺.

Highlights

- Neuronal ADP:ATP is not affected by neurotransmission despite strong Na⁺ pumping
- Stimulated mitochondrial pyruvate flux precedes glucose consumption
- Energy stability is not explained by conventional homeostasis (ADP:ATP or Ca²⁺)
- Na⁺ pump activity controls glycolysis and mitochondrial ATP production



Non-Canonical Control of Neuronal Energy Status by the Na⁺ Pump

Felipe Baeza-Lehnert,^{1,2} Aiman S. Saab,^{3,4} Robin Gutiérrez,^{1,2} Valeria Larenas,¹ Esteban Díaz,^{1,2} Melanie Horn,¹ Miriam Vargas,^{1,2} Ladina Hösli,^{3,4} Jillian Stobart,^{3,4} Johannes Hirrlinger,^{5,6} Bruno Weber,^{3,4} and L. Felipe Barros^{1,7,*}

¹Centro de Estudios Científicos (CECs), Casilla 1469, 5110466 Valdivia, Chile

²Universidad Austral de Chile, Valdivia, Chile

³Institute of Pharmacology and Toxicology, University and ETH Zurich, Switzerland

⁴Neuroscience Center Zurich, Zurich, Switzerland

⁵Carl-Ludwig-Institute for Physiology, Faculty of Medicine, University of Leipzig, 04103 Leipzig, Germany

⁶Department of Neurogenetics, Max-Planck-Institute for Experimental Medicine, Hermann-Rein-Str. 3, 37075 Göttingen, Germany

⁷Lead Contact

*Correspondence: fbarros@cecs.cl

<https://doi.org/10.1016/j.cmet.2018.11.005>

SUMMARY

Neurons have limited intracellular energy stores but experience acute and unpredictable increases in energy demand. To better understand how these cells repeatedly transit from a resting to active state without undergoing metabolic stress, we monitored their early metabolic response to neurotransmission using ion-sensitive probes and FRET sensors *in vitro* and *in vivo*. A short theta burst triggered immediate Na⁺ entry, followed by a delayed stimulation of the Na⁺/K⁺ ATPase pump. Unexpectedly, cytosolic ATP and ADP levels were unperturbed across a wide range of physiological workloads, revealing strict flux coupling between the Na⁺ pump and mitochondria. Metabolic flux measurements revealed a “priming” phase of mitochondrial energization by pyruvate, whereas glucose consumption coincided with delayed Na⁺ pump stimulation. Experiments revealed that the Na⁺ pump plays a permissive role for mitochondrial ATP production and glycolysis. We conclude that neuronal energy homeostasis is not mediated by adenine nucleotides or by Ca²⁺, but by a mechanism commanded by the Na⁺ pump.

INTRODUCTION

The brain consumes energy at a rate 10 times faster than the rest of the body. Over half of this energy is used by neuronal pumps to restore ion gradients challenged by excitatory synaptic potentials and action potentials (Erecinska and Silver, 1994; Harris et al., 2012). Neurons are unique insofar as they lack energy stores while being exposed to acute unpredictable increases in energy demand. It is not clear how these cells can transit from resting to active state time and again over a lifetime without undergoing metabolic stress. The details of such adaptive response seem particularly relevant because acute energy shortage has a quick and profound impact on brain cell function

and viability, as exemplified by hypoxia and hypoglycemia. Neurons may be particularly susceptible to small ATP deficits, with possible consequences for neurodegeneration (Le Masson et al., 2014; Zilberter and Zilberter, 2017).

ATP bridges the gap between energy usage by biochemical processes and energy production by mitochondria and glycolysis. The neuronal ATP pool is highly dynamic, with typical turnover times in the order of seconds (Barros et al., 2013). Different control systems contribute to balance energy demand and supply at different time scales. For example, the AMP-activated protein kinase takes minutes to signal the expression of proteins involved in fuel supply and ATP turnover (Hardie et al., 2012). Isotopic studies of purified enzymes and respirometry assays of isolated mitochondria suggested that mitochondrial respiration is controlled also in the short term by homeostatic feedback loops, in which ADP is the controlling variable (Chance and Williams, 1956; Brand and Nicholls, 2011). Accordingly, studies in intact cells and tissues reported fast depletion of ATP in response to energy demand and/or decreased fuel/oxygen delivery (Erecinska and Silver, 1994; Jekabsons and Nicholls, 2004; Connolly et al., 2014; Lange et al., 2015; Rangaraju et al., 2014; Toloe et al., 2014; Rueda et al., 2015), and therefore the control of mitochondrial respiration by adenine nucleotide feedback has become standard in mathematical models of cell metabolism (Aubert et al., 2007; Jolivet et al., 2015; Le Masson et al., 2014; Berndt et al., 2015). However, low-resolution measurements showed that bulk tissue ATP in skeletal muscle, heart, and brain is relatively insensitive to workload (Hill, 1950; Hochachka and McClelland, 1997; Heineman and Balaban, 1990; Du et al., 2008). These findings have prompted alternative hypotheses, namely that mitochondrial respiration is controlled by local adenine nucleotide pools (Saks et al., 2008) or by Ca²⁺, either intramitochondrial or cytosolic (Duchen et al., 2008; Glancy and Balaban, 2012; Denton, 2009; Llorente-Folch et al., 2013).

Genetically encoded fluorescence resonance energy transfer (FRET) reporters are allowing real-time measurement of metabolite concentrations and fluxes in intact cells and in minimally invasive fashion (Takanaga et al., 2008; Imamura et al., 2009; Bittner et al., 2010; Tantama et al., 2013; San Martín et al., 2013, 2014; Barros et al., 2013; Diaz-Garcia et al., 2017). Taking advantage of these tools in combination with ion-sensitive dyes



and a novel protocol to evaluate ATP flux in real-time, we have approached the question of short-term control of energy metabolism in neurons.

RESULTS

To study the energetics of neurotransmission, we first used cultured neurons, which provide precise control of experimental variables and easier visualization of dyes and sensors. Neurons were cultured in the presence of astrocytes (Figure S1A), which promote their functional and metabolic differentiation (Barres et al., 1990; Mamczur et al., 2015).

Resting Hippocampal Neurons Consume Both Glucose and Lactate

It is well established that neurons consume glucose but the role of lactate as fuel is contentious (Pellerin and Magistretti, 1994; Barros and Weber, 2018; Bak and Walls, 2018). Here, we addressed this issue with the FRET sensor Laconic and a transport-stop protocol based on the monocarboxylate transporter (MCT)1-2 blocker AR-C155858 (Figures S1B–S1D; San Martín et al., 2013). In the presence of physiological concentrations of glucose and lactate, the majority of neurons behaved as lactate consumers, whereas all astrocytes were lactate producers (Figures S1B and S1C). Additional characterization showed that as the cultures became more mature, the transport and consumption of glucose diminished in neurons and increased in astrocytes and that astrocytic enrichment of the cultures reduced the consumption of glucose by neurons (Figures S1E–S1L). Thus, under our experimental conditions, both glucose and lactate contribute to the fueling of neurons.

Neurotransmission was triggered by field stimulation of the cultures with a short theta burst (STB, Figure 1A), an electrical stimulation protocol of 40 pulses in a pattern that resembles hippocampal activity (Albensi et al., 2007). The STB elicited a Ca^{2+} signal of similar amplitude to that produced by spontaneous firing (Figure 1B). The cytosolic Ca^{2+} transient peaked 4 s after stimulation onset, lasted for 20 s, was strongly inhibited by a cocktail of DNQX and MK801, and was abolished by TTX (Figures 1C–1F), demonstrating predominant glutamatergic neurotransmission driven by action potentials. Using the high-affinity probes Rhod2 or mito-GCaMP6s (Li et al., 2014), we did not find sizable increases in intramitochondrial Ca^{2+} in response to the STB (Figures 1G–1J).

Quantitation of the Workload Elicited by Synaptic Activity

The cytosolic Ca^{2+} transient was accompanied by a much slower Na^+ transient that peaked at 30 s and lasted for several minutes (Figure 2A). The Na^+ transient was similar in amplitude and time course to spontaneous Na^+ fluctuations recorded in brain tissue slices (Rose and Ransom, 1997), as detected with Na^+ -binding benzofuran isophthalate (SBFI) or Asante Sodium Green probes (Figure S2). Both Ca^{2+} and Na^+ transients could be elicited repeatedly in the same preparation (Figure S2). The return of Na^+ toward pre-stimulation levels reveals a metabolic load, but the extent of the load may not be computed directly from the Na^+ concentration curve, because of unknown simultaneous contributions from Na^+ influx and pumping (as exemplified in Fig-

ure S3A). To circumvent this limitation, a protocol was devised based on Na^+ pump blockage. Figures 2A and 2B show that the curves of Na^+ accumulation with and without ouabain were virtually superimposable during the first 15 s after STB onset and sharply diverged afterward. The difference between the two curves was computed as Na^+ extruded, and its instant slope as the rate of extrusion, that is, the activity of the Na^+ pump (Figure 2C). One limitation of this approach is that the accumulation of intracellular Na^+ may interfere with the influx of Na^+ , for example via the $\text{Na}^+/\text{Ca}^{2+}$ exchanger, a possibility supported by the observation that cytosolic Ca^{2+} did not return to control levels after the STB in the ouabain-treated cells (Figure S3B). Therefore, to minimize underestimation of the rate of Na^+ pumping, analyses were restricted to the first 30 s after stimulation, a period in which Na^+ levels are still in the low millimolar range. Neuronal pH was not affected by the STB, either in the absence or presence of ouabain (Figure S3C), which is against a confounding effect of the Na^+/H^+ exchanger.

To determine the relative importance of Na^+ pumping on overall ATP expenditure, glucose metabolism was measured using a transport-stop protocol based on the FRET sensor FLII¹² Pglu700 $\mu\Delta$ 6 (see schematic in Figure 4E; Takanaga et al., 2008; Bittner et al., 2011). The rate of glucose consumption by resting neurons was 0.8 $\mu\text{M}/\text{s}$ in the presence of lactate and 1.7 $\mu\text{M}/\text{s}$ in its absence, with a negligible change in cytosolic ADP:ATP after lactate removal (Figures S4B and S4C). As lactate has been shown to sustain *in vivo* neurotransmission as well as does glucose (Wyss et al., 2011), we assumed that the sum of glucose and lactate amounted to 1.7 $\mu\text{M}/\text{s}$ of glucose equivalents, that is, that lactate contributes about 50% of resting fuel (Bouzier-Sore et al., 2006). With a stoichiometry of 31 ATPs per glucose, this fueling rate translated into an ATP production of 53 $\mu\text{M}/\text{s}$. Considering the measured Na^+ pumping rate of 46 $\mu\text{M}/\text{s}$ (Figure 2A), and a 3:1 $\text{Na}^+:\text{ATP}$ stoichiometry, the resting ATP consumption of the Na^+ pump was 15 $\mu\text{M}/\text{s}$. We conclude that housekeeping functions in these cells consumed ATP at a rate of 38 $\mu\text{M}/\text{s}$ (from 53 $\mu\text{M}/\text{s}$ minus 15 $\mu\text{M}/\text{s}$). Taken together, the Na^+ and glucose measurements show that a moderate level of neurotransmission stimulated neuronal ATP consumption to a large extent, from 53 $\mu\text{M}/\text{s}$ to a maximum 155 $\mu\text{M}/\text{s}$, an increase of 1.9 fold (Figures 2D and S4D). Still, this figure is an underestimate, as neurotransmission also involves ATP usage by minor processes such as Ca^{2+} pumping, synaptic vesicle recycling, and actin remodeling (Harris et al., 2012).

Invariance of Cytosolic ATP and ADP and Estimation of ATP Production

How the large increase in ATP expenditure brought about by synaptic activity impacts the energy status of neurons was first gauged using the genetically encoded ATP sensor ATeam 1.03 (Imamura et al., 2009). According to a mathematical simulation based on the conventional homeostatic model of ADP feedback with a Hill coefficient of 1 (see STAR Methods), the estimated 1.9-fold rise in ATP demand should have resulted in substantial depletion of the cytosolic ATP pool. However, experiments showed no detectable change (Figure 3A). With ATP as constant, an estimated cytosolic ADP was obtained with the ADP:ATP reporter Perceval high range (HR) (Tantama et al., 2013). Again, the ADP:ATP ratio was unaffected by the STB (Figure 3B), showing

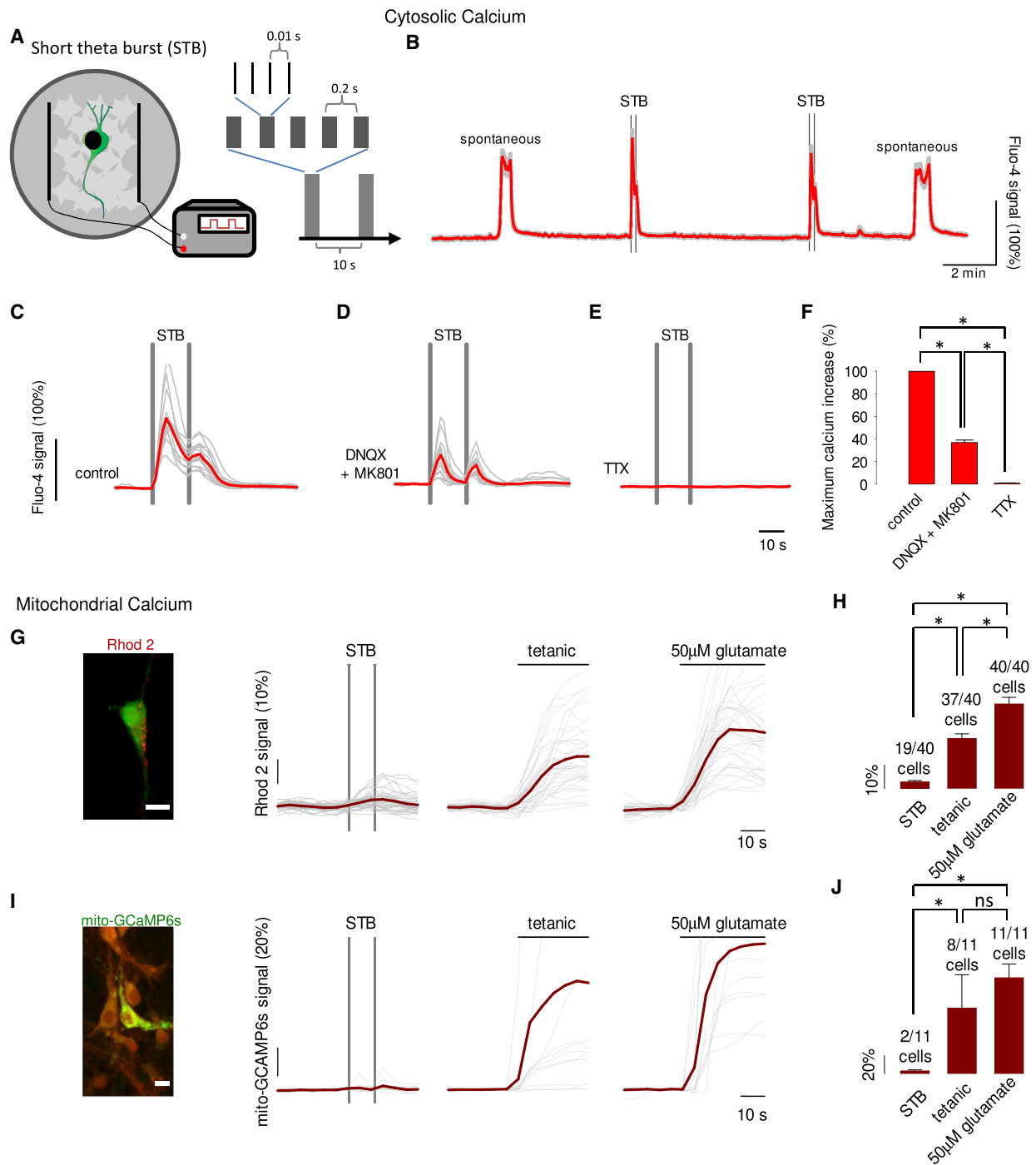


Figure 1. Cytosolic and Mitochondrial Ca^{2+} in Response to Neurotransmission

(A) Field stimulation of mixed hippocampal cultures with a short theta burst (STB) protocol (see details in STAR Methods).

(B) The response of neuronal Ca^{2+} to STB stimulation was monitored in Fluo4-loaded cultures. Spontaneous Ca^{2+} transients are indicated. Mean \pm SEM (17 cells).

(C–E) Ca^{2+} responses to STB under control conditions (C), in the presence of 30 μ M DNQX and 15 μ M MK801 (D), or in the presence of 2 μ M TTX (E). Individual traces from 17 cells (gray), with averages in bold (red).

(F) Summary of three experiments similar to that shown in (C–E). Mean \pm SEM (43 cells, *p < 0.05).

(G and I) The response of mitochondrial Ca^{2+} to STB stimulation, tetanic stimulation (20 Hz for 30s) and 50 μ M glutamate was monitored in cells loaded with Rhod-2 (G, 49 cells in three experiments) or mito-GCaMP6s (I, 11 cells in eleven experiments). Insets show a neuron loaded with Rhod-2 (red) and Calcein (green), and a neuron expressing mito-GCaMP6s (green) in a culture loaded with Calcein Orange (red). Bars represent 10 μ m.

(H and J). Summary of amplitudes (mean \pm SEM) of the Rhod-2 (H) and mito-GCaMP6s (J) responses to STB, tetanic and glutamate. The number of responsive cells is indicated on top of each bar. Mean \pm SEM; *p < 0.05.

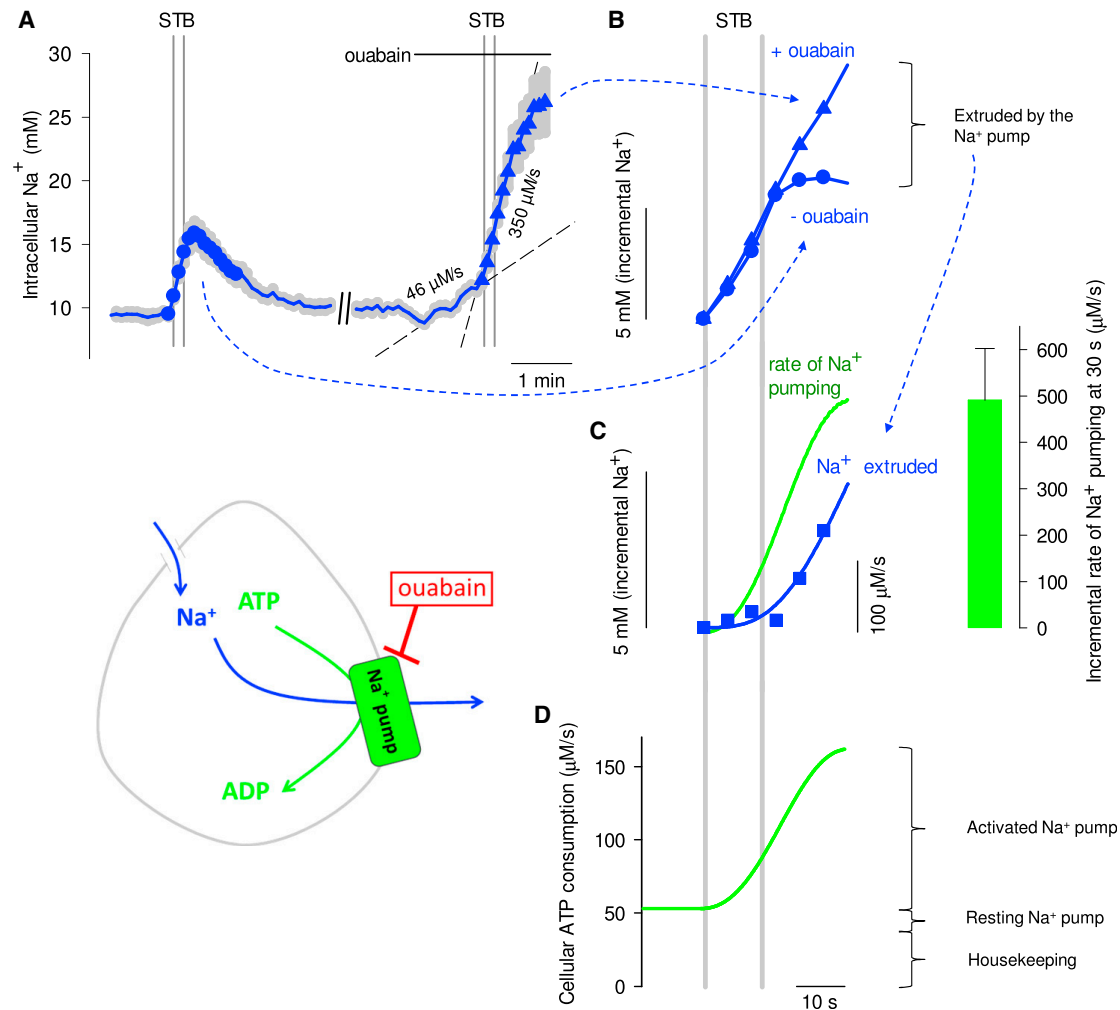


Figure 2. Quantification of the Metabolic Load Triggered by Neurotransmission

(A) The response of neuronal Na^+ concentration to STB stimulation under control conditions (circles) and in presence of 0.1 mM ouabain (triangles) was estimated with SBFI. Mean \pm SEM (10 cells from a single experiment). Na^+ accumulation rates reflecting Na^+ entry (interrupted lines), were estimated before and after STB. (B) The time courses of Na^+ accumulation induced by the STB in the absence (circles) and presence of 0.1 mM ouabain (triangles) are plotted together. Note the divergence between the two time courses, attributed to Na^+ pumping.

(C) The amount of Na^+ extruded (squares) was calculated as the point-by-point difference between Na^+ accumulation in the absence and presence of 0.1 mM ouabain illustrated in (B). The continuous blue line corresponds to the fitting of three-parameter logistic curve to the data, $r^2 > 0.99$. The green curve shows the instant rate of Na^+ extrusion calculated as the first derivative of the Na^+ extrusion curve. The bar graph summarizes data from four experiments (27 cells), including the one illustrated in (A) and (B).

(D) The total rate of neuronal ATP consumption was obtained by adding the ATP consumption related to Na^+ pumping (from C) to the ATP consumption devoted to housekeeping functions, estimated from the rate of glucose consumption (Figure S4).

that cytosolic ADP is also insensitive to synaptic activity. Similar changes in adenine nucleotides were predicted by an alternative feedback model based on explicit set points (Figure S5; Le Masson et al., 2014). A possible confounding effect of pH on Perceval HR (Tantama et al., 2013) was ruled out as the STB did not affect cytosolic pH in these cells to a measurable extent (Figures S3C and S5C). The large responses of both ATeam and Perceval HR to OXPHOS inhibition (Figures 3A, 3B, and S5) and to supra-physiological stimulation (see below), confirm previous reports that neuronal ATP and ADP concentrations lie in the sensing range of the probes (Imamura et al., 2009; Rangaraju et al., 2014; Toloe et al., 2014; Lange et al., 2015). No ADP:ATP change

was detected in cells fueled exclusively with lactate (Figure S6), although there was a small but statistically significant change in glucose fueled cells. These results confirm that neurons may signal efficiently in either substrate and that a robust glycolytic flux in neurons is not necessary for neuronal energy homeostasis, at least in the short term (Wyss et al., 2011).

The stability of cytosolic ATP was very informative, as it revealed that ATP consumption by the Na^+ pump is matched, second-by-second, by a commensurate increase in ATP production, defined as the release of ATP to the cytosol (Figure 4C). The invariance also suggested that ATP and ADP may not account for the tight coupling between ATP demand and

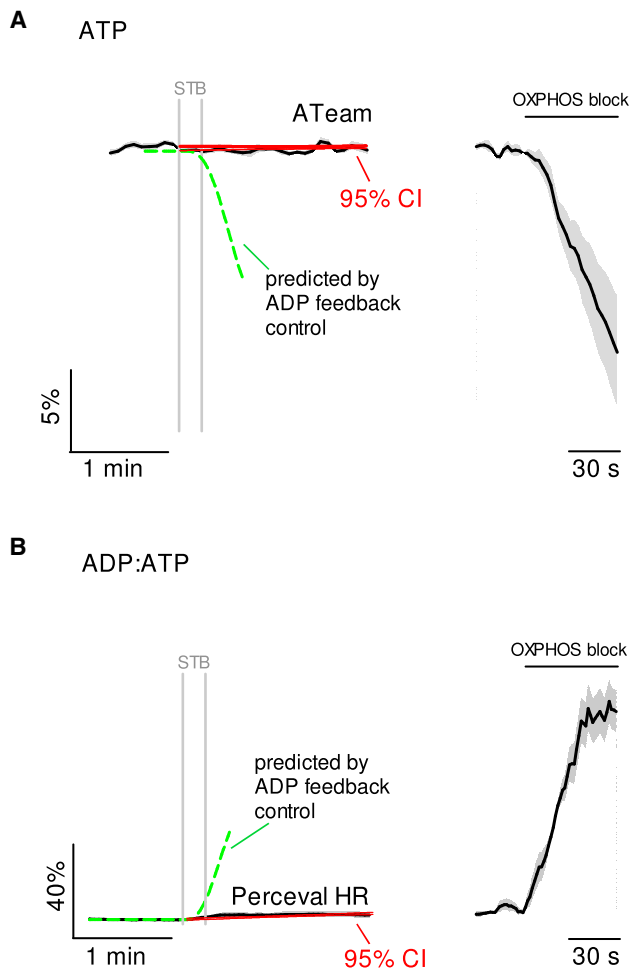


Figure 3. Invariance of Neuronal ATP and ADP after Neurotransmission

(A) Left, ATP response to STB stimulation measured with ATeam. Mean \pm SEM (16 cells in ten experiments, black line). The interrupted green line shows a mathematical simulation of the response as it should have been observed with ATeam in cell governed by a negative feedback controlled by ADP. Right, effect of OXPPOS blockage with 5 mM azide on ATP as measured with ATeam. Mean \pm SEM (16 cells in ten experiments). The 95% confidence interval (CI) of the mean is shown.

(B) Left, ADP:ATP ratio response to STB stimulation measured with Perceval HR. Mean \pm SEM (15 cells in 15 experiments, black line). The interrupted green line shows a mathematical simulation of the response as it should have been observed with Perceval HR in cell governed by a negative feedback controlled by ADP. Right, Effect of OXPPOS blockage with 5 mM azide on ADP:ATP ratio as observed with Perceval HR. Mean \pm SEM (15 cells in 15 experiments). The 95% confidence interval (CI) of the mean is shown.

production, a conclusion substantiated by a sensitivity analysis based on numerical simulation (Figure S6). For example, to account for the observed energy invariance, the stimulation of Na^+ pumping would have to be less than a 10th of what was measured or, reciprocally, resting ATP consumption would have to be more than 10 times larger than that estimated. These two unfavorable scenarios are not only inconsistent with our measurements, but also with the relative weight of signaling versus housekeeping in the neuronal energy budget (Harris

et al., 2012) and with the strong stimulation of glucose and pyruvate consumption by STB described below. Alternatively, mitochondria would have to sense [ADP] with a Hill coefficient of >100 , way beyond the reported range of 1–4 (Wilson, 2017). Figure S6 also shows that even a 1-s delay between Na^+ pumping and ATP production would lead to detectable fluctuations in ATP and ADP. Neurons possess substantial levels of phosphocreatine in equilibrium with the ATP pool (Hertz et al., 1988; Jolivert et al., 2015). As this pool is a fixed reservoir, it slightly slows down the onset of the predicted ATP depletion but does not change its amplitude (Figure S7). The predicted time course of AMP, phosphocreatine and other metabolites in response to the STB is shown in Figure S7.

Early Metabolic Responses to Synaptic Activity

The cytosolic pools of pyruvate, lactate, and glucose were unperturbed by the STB (Figures 4A and 4B). However, when transport-stop protocols (Bittner et al., 2010; San Martín et al., 2014) were applied, large underlying changes in metabolic fluxes became visible. The stimulation of mitochondrial pyruvate uptake was immediate (Figures 4C and 4D). The median stimulation of pyruvate consumption was 2.6-fold and showed a half-time of 4 s, much shorter than that of stimulated ATP production (18 s; Figure 4G), revealing that mitochondria accumulate energy in some form before releasing ATP to the cytosol. Electrical stimulation of neurons is known to induce a biphasic change in mitochondrial NAD(P)H autofluorescence, characterized by a fast transient dip (oxidation) and a secondary overshoot (reduction) in which autofluorescence surpasses the baseline (Shuttleworth, 2010). The early phase of mitochondrial energization together with the delayed production of ATP described here, may provide an explanation for the overshoot phase of NAD(P)H autofluorescence. The consumption of glucose was also stimulated by synaptic activity, with a median of 1.9-fold, and its onset was delayed with respect to mitochondrial pyruvate uptake (Figures 4E and 4F). This first direct demonstration of glycolysis stimulation by neurotransmission provides a straightforward explanation for the rise in cytosolic NADH/NAD⁺ measured in hippocampal slice neurons, which also peaked about 30 s after the onset of synaptic activity (Diaz-Garcia et al., 2017). It is not possible at this stage to tell how much of the stimulated glucose flux was diverted through the pentose phosphate pathway (Herrero-Mendez et al., 2009). The delay between pyruvate uptake and glucose consumption implies that the pyruvate pool is sustained by lactate, at least during the first 10 to 20 s in which glycolysis has not been fully activated. A limitation of the present mitochondrial pyruvate uptake assay is that it requires the absence of glucose. Activation of the malate-aspartate shuttle (MAS) by Ca^{2+} may control the utilization of glycolytic pyruvate (Llorente-Folch et al., 2013), which may not start at the same time as that of external pyruvate.

Control of Mitochondrial ATP Production by the Na^+ Pump

The two signals that have been involved in the control of mitochondrial ATP production by workload are cytosolic ADP and Ca^{2+} , both intramitochondrial (Glancy and Balaban, 2012; Denton, 2009) and cytosolic (Llorente-Folch et al., 2013; Gellerich et al., 2013). As shown in Figures 1G–1J, only a small increase

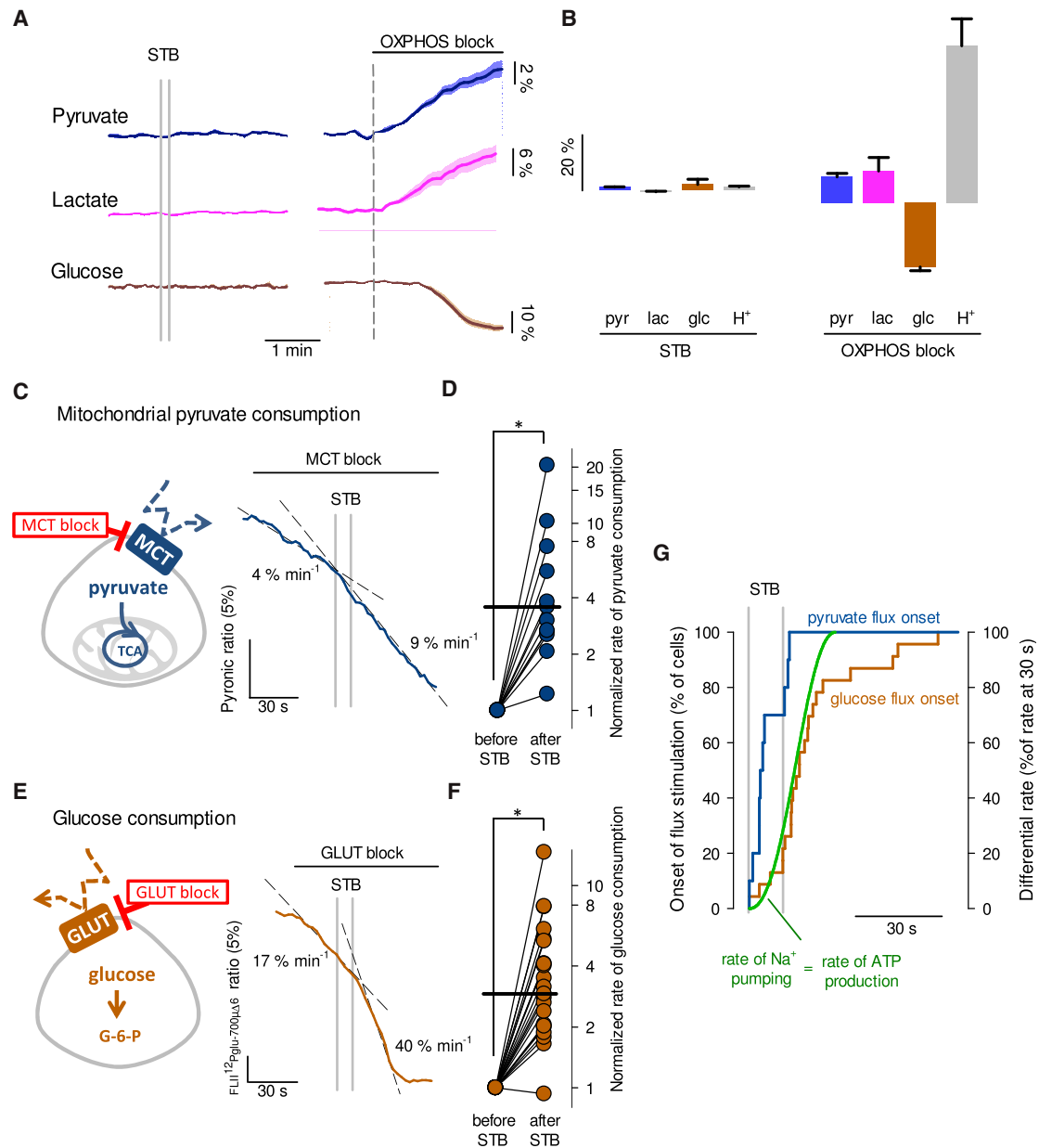


Figure 4. Metabolic Response to Neurotransmission

(A) Left, effect of STB on the levels of pyruvate, lactate and glucose in neurons superfused with 2 mM glucose and 1 mM lactate. Right, effect of OXPHOS blockage with 5 mM azide. Mean \pm SEM.

(B) Summary of the data in (A), showing in the left graph the change induced by the STB for pyruvate (pyr, 10 cells in six experiments), lactate (lac, 9 cells in eight experiments), glucose (glc, 8 cells in three experiments) and H⁺ concentration (24 cells in three experiments). Right, summary of the data for the effect of OXPHOS inhibition with 5 mM azide on pyruvate (7 cells in four experiments), lactate (6 cells in three experiments), glucose (16 cells in four experiments) and H⁺ concentration (24 cells in three experiments). Mean \pm SEM.

(C) Effect of STB on the rate of mitochondrial pyruvate consumption as measured with a transport-stop protocol based on the MCT blocker AR-C155858 (1 μ M), in the presence of 400 μ M extracellular pyruvate and absence of glucose and lactate. Rates were obtained by linear regression using the points preceding the STB (resting) or starting 30 s after the onset of the STB (stimulated).

(D) Mitochondrial pyruvate consumption rates before and after STB stimulation (13 neurons in seven experiments). The median stimulation of the rate is represented by a thick horizontal line. *p < 0.05.

(E) Effect of STB on the rate of glucose consumption as measured with a transport-stop protocol based on the GLUT blocker cytochalasin B (20 μ M), in the presence of 2 mM glucose and 1 mM lactate. Rates were obtained by linear regression using the points preceding the STB (resting) or starting 30 s after the onset of the STB (stimulated).

(legend continued on next page)

in mitochondrial matrix Ca^{2+} was observed in response to the STB. A larger mitochondrial Ca^{2+} increase was elicited by tetanic stimulation (20 Hz for 30 s), but this resulted in inhibition of mitochondrial pyruvate influx (Figure S7). This was in register with a reduced pyruvate-fueled respiration by intramitochondrial Ca^{2+} (Gellerich et al., 2013; Pandya et al., 2013). Mitochondrial metabolism is sensitive to cytosolic Ca^{2+} via proteins that expose Ca^{2+} -binding sites to the mitochondrial intermembrane space, such as the aspartate/glutamate transporter ARALAR, a key component of the MAS (Llorente-Folch et al., 2013). However, the time courses of both cytosolic and mitochondrial Ca^{2+} preceded that of ATP production (Figure 5A). Although there was a good correlation between ATP production and cytosolic Na^+ (Figure 5A), mild Na^+ elevations caused by pharmacological or functional inhibition of the Na^+ pump (Figure 2A) did not increase neuronal ATP (Figure 5B), despite reduced ATP usage. Moreover, the large Na^+ elevation triggered by the STB in the presence of ouabain (Figure 2A) also failed to stimulate ATP production (Figure 5C). While discarding a direct role for Na^+ , these results demonstrate that mitochondrial ATP production requires an active Na^+ pump. Consistently, a reduction of the Na^+ load triggered by the STB did not affect the coupling between ATP usage and production (Figure 5D). The neuronal Na^+ pump was also found to play a permissive role over glycolysis, a phenomenon previously described in astrocytes (Pellerin and Magistretti, 1994, 1997; Bittner et al., 2011). These findings suggest that mitochondrial and glycolytic ATP production in neurons is controlled by Na^+ via the Na^+ pump (Figure 5F).

ATP Invariance in Cortical Neurons *In Vivo*

Next, ATP dynamics were investigated in neurons of the somatosensory cortex using B6-Tg(Thy1.2-A_{Team}1.03^{YEMK^AJhi}), a transgenic mouse expressing A_{Team} under the Thy1 promoter (Trevisiol et al., 2017), and two-photon imaging (Figure 6A). Under light anesthesia, neurons displayed considerable spontaneous activity as evidenced by the Ca^{2+} -sensitive sensor RCaMP1.07, but parallel recordings in A_{Team} mice showed no detectable ATP fluctuations (Figure 6B). The Ca^{2+} activity increased in response to whisker stimulation but again, no ATP changes were observed (Figure 6C). The sensitivity of the sensor *in vivo* was illustrated by direct electrical stimulation of the tissue, which produced a much larger Ca^{2+} signal, and was accompanied by a significant drop in ATP that depended on both frequency (Figure 6E) and intensity (Figure 6F). These observations showed that ATP consumption and mitochondrial ATP production are also tightly coupled *in vivo*.

To investigate the dynamic range of the novel homeostatic system, cultured neurons were exposed to graded workloads. Direct exposure to glutamate, which induced maximum increases in cytosolic Na^+ and Ca^{2+} , as well as in mitochondrial Ca^{2+} (Figure 7A), resulted in substantial depletion of ATP (Figure 7B), an effect likely compounded by inhibition of glucose

transport by glutamate (Porrás et al., 2004; Tesccarollo et al., 2014). Intermediate workloads were applied by changing the number of electric pulses or by applying NMDA. The changes in ATP and ADP:ATP ratio were plotted as a function of the cytosolic Ca^{2+} increase, used as a proxy of the ATP demand (Figure 7C). This representation, together with the inhibition of mitochondrial pyruvate uptake by tetanic stimulation (Figure S7) suggests that in cultured hippocampal neurons, the workload imposed by the STB is near the maximum that may be tolerated without metabolic stress.

DISCUSSION

We have addressed the fundamental question of how neurons adapt to workload, using technologies that allowed a quantitative survey of the first seconds that follow neurotransmission. Our main conclusion is that mitochondrial ATP production in neurons is exquisitely regulated by the Na^+ pump, but not via adenine nucleotides or Ca^{2+} , at least in response to moderate levels of synaptic activity. Other important findings were the joint consumption of glucose and lactate by resting neurons, the stimulation of both pyruvate flux and glucose flux by synaptic activity and a “priming” phase of mitochondrial energization that precedes the production of ATP.

Control of Mitochondrial ATP Production

Neurotransmission is well suited to the study of fast metabolic coupling because a strong ATP flux occurs in a predictable fashion between a single identified source (mitochondria) and a single identified sink (Na^+ pump), which can be manipulated in graded fashion. Our conclusions rest on the following: (1) *Quantitation of ATP consumption*. By monitoring the activity of the Na^+/K^+ ATPase and glucose consumption in real time, we made it possible, for the first time, to estimate the flux of ATP. (2) *Detection of ADP:ATP*. Being one order of magnitude smaller than the ATP pool, the ADP pool sustains the same flux, which makes it much more sensitive to possible mismatches between source and sink. The combination of no detectable ATP changes with invariance of Perceval HR and cytosolic pH revealed that ADP was also stable. This is important because OXPHOS is thought to be controlled by ADP, the levels of which had not been hitherto accessible. (3) *Spatiotemporal resolution*. Transient changes may be missed by low resolution techniques such as MRS, which need extended integration times and average the behavior of many cells, a particular concern for heterogeneous tissues like brain. (4) *Physical separation between ATP source and ATP sink*. The existence of metabolite microdomains has been hypothesized in skeletal muscle, where mitochondria are close to contractile elements (Saks et al., 2008). Mitochondria can also make contact with the plasma membrane (Westermann, 2015), but most of them are buried within the cell (Deitch and Banker, 1993), whereas most Na^+ pumps reside at the cell surface (Juhászová and Blaustein, 1997). This separation

(F) Glucose consumption rates before and after STB stimulation (23 neurons in ten experiments). The median stimulation of the rate is represented by a thick horizontal line. * $p < 0.05$.

(G) Onset of pyruvate (13 cells, blue) and glucose (23 cells, brown) flux stimulations. The onset was estimated for each cell as the intercept between linear regressions fitted to the data before and after the STB, as explained in (C) and (E). As a reference, the rates of stimulated Na^+ pumping/ATP production are shown in green (from Figure 2C plus ATP invariance).

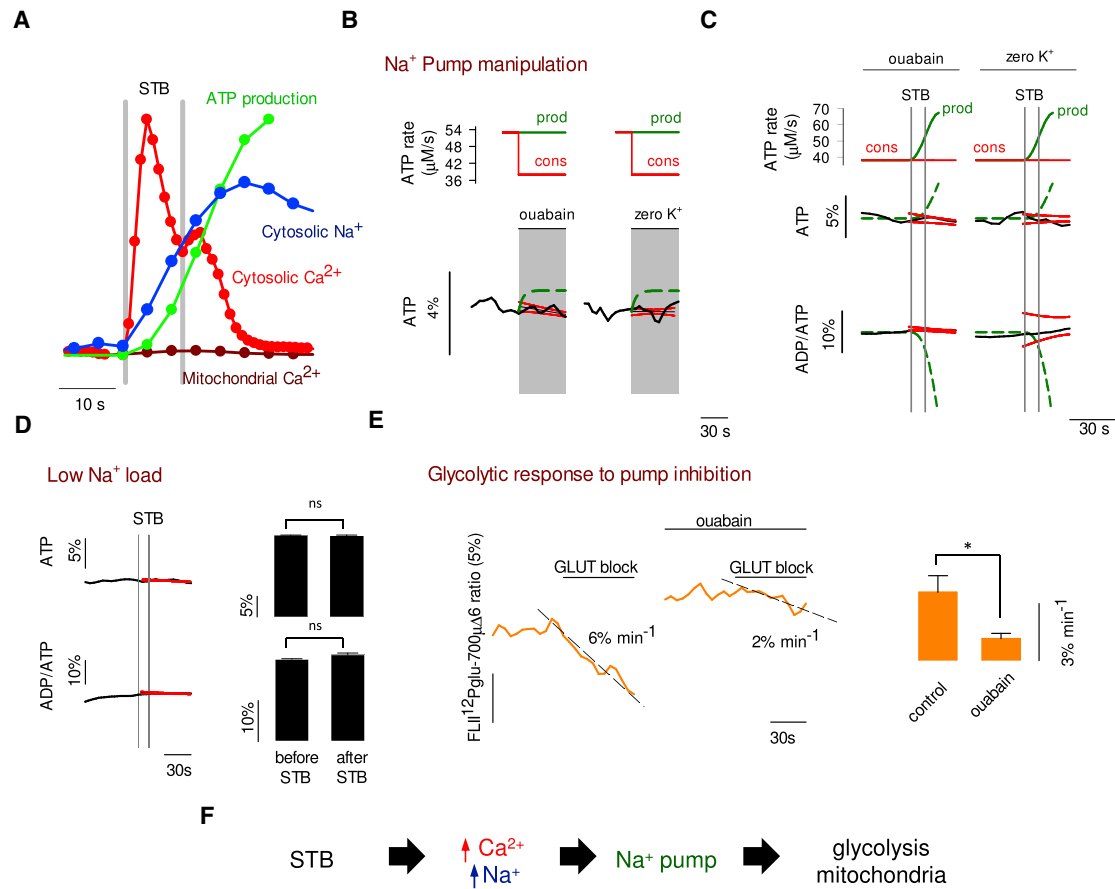


Figure 5. Na^+ Pump Involvement in Activity-Metabolism Coupling

(A) Time courses of cytosolic Ca^{2+} (from Figure 1C), mitochondrial Ca^{2+} (from Figure 1I), cytosolic Na^+ (from Figure 2A), and ATP production (from Figure 4G). Vertical scales are arbitrary.

(B) Effect of direct manipulation of Na^+ pump activity on ATP. Top, expected impact of full Na^+ pump blockage on neuronal ATP consumption (cons) and Na^+ pump-independent production (prod). Bottom, mean ATP levels measured with ATeam in response to 0.1 mM ouabain (nine cells in seven experiments) or zero extracellular K^+ (ten cells in ten experiments); 95% confidence intervals are shown in red. Predicted changes in ATP level are shown as broken green lines.

(C) Effect of STB on ATP and ADP:ATP ratio in the absence of Na^+ pump activity. Top, expected impact of STB on neuronal ATP consumption (cons) and Na^+ pump-independent production (prod). Bottom, mean traces for cells pre-incubated for 1 min in 0.1 mM ouabain (ATeam: nine cells in seven experiments. Perceval HR: nine cells in nine experiments), or zero K^+ (ATeam: ten cells in ten experiments. Perceval HR: ten cells in ten experiments). 95% confidence intervals are shown in red. Predicted changes in ATP and ADP:ATP ratio are shown as broken green lines.

(D) Cells were stimulated in the presence of 80 mM extracellular Na^+ , equimolarly replaced with N-methyl-D-glucamine (ATeam: eight cells in eight experiments. Perceval HR: nine cells in eight experiments). Bars represent readings before and after the STB (mean \pm SEM; ns, $p > 0.05$).

(E) Glucose consumption was measured in the absence and presence of 0.1 mM ouabain. Bars represent the results of 13 neurons in six experiments (mean \pm SEM; * $p < 0.05$).

(F) Proposed sequence of metabolic control in neurons.

means that the crosstalk between Na^+ pump and mitochondria can be accurately monitored with sensors interposed in the bulk cytosol. Incidentally, according to Brownian diffusion the cytosol of mammalian cells is a well-mixed compartment for ATP and ADP, even in the immediate vicinity (1 nanometer) of sinks and sources (Barros and Martinez, 2007). With quantitative knowledge of metabolite levels and fluxes in real time, it was possible to rule out adenine nucleotides as mediators of the energetic adaptation to synaptic activity.

The alternative candidate for activity-dependent control of mitochondrial metabolism has been Ca^{2+} (Duchen et al., 2008; Glancy and Balaban, 2012; Tarasov et al., 2012; Llorente-Folch et al., 2013). Ca^{2+} may regulate mitochondrial metabolism by

acting on matrix dehydrogenases or at the cytosolic side of mitochondrial transporters. The current finding of substantial stimulation of pyruvate uptake and ATP production without significant increases in matrix Ca^{2+} argues against a necessary role for this cation in the control of neuronal energetics, at least in the short term. Moreover, mitochondrial Ca^{2+} was not correlated with ATP production in response to the STB, whereas a larger increase in mitochondrial Ca^{2+} induced by tetanic stimulation resulted in inhibition of pyruvate consumption. Matrix dehydrogenases require micromolar Ca^{2+} , and it is not clear that respiration can be stimulated by Ca^{2+} when fed with pyruvate, the physiological substrate for dehydrogenases in neurons (Gellerich et al., 2013; Pandya et al., 2013). It was recently reported that

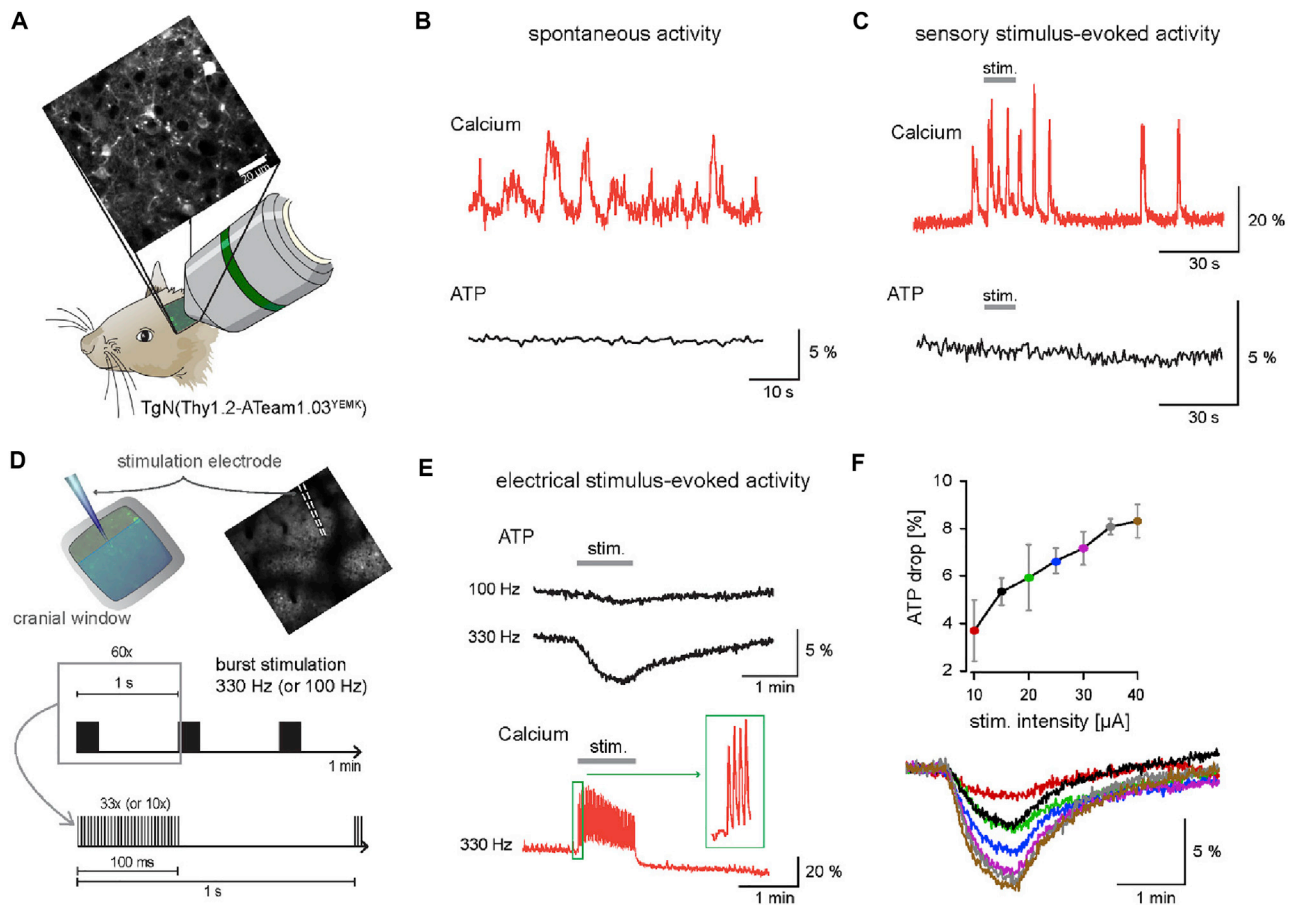


Figure 6. ATP Invariance In Vivo

(A) *In vivo* two-photon imaging of neuronal ATP levels in B6-Tg(Thy1.2-ATeam1.03^{YEMK})_{A^{hi}}. Bar represents 20 μ m. (B–F) In addition to ATP levels, neuronal activity was monitored by calcium imaging using RCaMP1.07 (Ohkura et al., 2012) cortically expressed by viral-mediated delivery (AAV9-hSYN-RCaMP1.07). (B) ATP levels (lower trace) were unchanged during spontaneous activities revealed by calcium transients (upper trace). (C) Sensory-evoked activity following electrical whisker-pad stimulation (2 Hz for 10 s, at 400 μ A) showed clear calcium responses in neurons, although ATP levels remained unchanged. (D) Scheme for microelectrode insertion and intracortical stimulation (top row). Burst stimulation paradigm for 1 min (1 Hz burst frequency, 100 ms trains at 100 or 330 Hz). (E) ATP level changes (top) in response to burst stimulations of 100 or 300 Hz (each at 15 μ A). Local microstimulations evoke robust calcium transients (bottom). Depicted are example traces. (F) Average ATP level changes following 1 min burst stimulation of 330 Hz at different current intensities ($n = 3$ mice, mean \pm SEM). Lower traces represent example recordings for each corresponding stimulus intensity (color-coded).

a major fraction of the 2-oxoglutarate dehydrogenase expressed in brain cells is insensitive to Ca^{2+} (Denton et al., 2016). ARALAR, a key component of the MAS, is sensitive to cytosolic Ca^{2+} in the nanomolar range, and should have been activated during the Ca^{2+} transient elicited by the STB. The modulation of ARALAR by Ca^{2+} is direct and reversible, and therefore expected to follow the kinetics of Ca^{2+} . Considering the divergent time courses of cytosolic Ca^{2+} and ATP production, a major role for the MAS in controlling ATP production is hard to envisage, although it likely contributes to mitochondrial energization.

Control of the ATP Source by the ATP Sink

How is information conveyed between synaptic activity and mitochondria? The dynamics of a putative signal responsible for matching ATP production to ATP consumption should mimic the complex time course of Na^+ pumping, including delay, rapid rise, and slow return to resting level. This was certainly not the

behavior of ATP, ADP, Ca^{2+} , or even Na^+ . Perfect correlation between stimulated Na^+ pumping and ATP production and instant adjustment of mitochondrial ATP production to Na^+ pump inhibition suggests that the top controller is the Na^+ pump itself. But how could the Na^+ pump modulate mitochondria if not via adenine nucleotides? One possible clue may be found in the striking coincidence between the time courses of Na^+ pumping and glycolysis (Figure 4E). In brain cells, the rate-limiting glycolytic enzyme hexokinase is attached to mitochondria, where it interacts with several proteins including the adenine nucleotide translocator ANT, the transporter in charge of ATP export to the cytosol (Genda et al., 2011). Whereas the functional role of this hexokinase location is unclear, its forced relocation to the cytosol has been associated with neurodegeneration (Hauser et al., 2017). There is ample evidence that the Na^+ pump plays a permissive role in glycolysis of astrocytes (Pellerin and Magistretti, 1994; Bittner et al., 2011; Fernandez-Moncada and Barros,

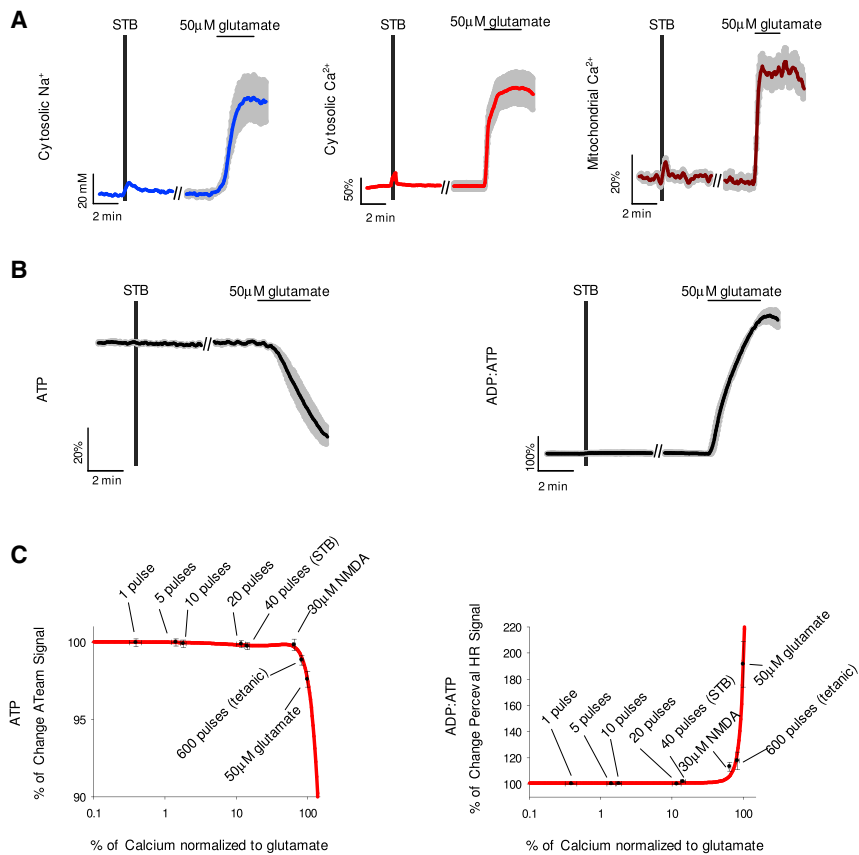


Figure 7. Supraphysiological Metabolic Uncoupling

(A) Comparison between the effects of STB and 50 μM glutamate on cytosolic Na^+ (10 cells), cytosolic Ca^{2+} (19 cells) and mitochondrial Ca^{2+} (15 cells). Mean \pm SEM, representative of more than three experiments per parameter.

(B) Comparison between the effects of STB and 50 μM glutamate on ATP (eight cells) and ADP:ATP ratio (ten cells). Mean \pm SEM, representative of more than eight experiments per parameter.

(C) Neurons were stimulated with an increasing number of electric pulses or exposed to 30 μM NMDA or 50 μM glutamate, while measuring intracellular Ca^{2+} , ATP or ADP:ATP. The plots express the change in nucleotide levels as a function of the maximum Ca^{2+} increase evoked in at least six experiments per stimulation protocol. Mean \pm SEM.

2014), specifically the minority $\alpha 2$ subunit of the pump (Pelierin and Magistretti, 1997), which is also expressed by neurons (Dobretsov and Stimers, 2005). A possible role for $\alpha 2$ is consistent with the high sensitivity of glutamate transport to ouabain and the physical interaction between glutamate transporters, the Na^+ pump, hexokinase, and the mitochondrial ATP exporters ANT and VDAC (Rose et al., 2009; Genda et al., 2011). Conceivably, the pump may regulate mitochondria through hexokinase and/or through the downstream glycolytic intermediates glucose-6-phosphate and fructose-1,6-bisphosphate (Diaz-Ruiz et al., 2008). Alternatively, the modulation may be direct, as neurons have invaginations of the plasma membrane that penetrate deep into the cytoplasm (Morris et al., 2003), plus there is a subpopulation of Na^+ pumps within the cell (Juhászová and Blaustein, 1997; Blom et al., 2011), some of which have been found in association with mitochondria (Hashimoto et al., 2008).

A Priming Phase of Mitochondrial Activation

The delay observed between stimulation of pyruvate consumption and ATP production means that the response to workload occurs in two steps: a priming phase, in which the organelle is energized, and an export phase, in which ATP is released “on demand” to the cytosol through the ANT. The priming phase explains why in the first seconds of activation there is an accumulation of reducing equivalents in mitochondria, visualized as the NADH overshoot (Chance and Williams, 1956; Shuttleworth, 2010) and may also help to explain the persistence of the

NADH overshoot in the presence of the ATP synthase blocker oligomycin (Duchen, 1992). Putting together the available data, we propose the following timeline: first, synaptic activity stimulates OXPHOS, possibly via cytosolic Ca^{2+} (Fein and Tsacopoulos, 1988) and causes the initial “dip” in matrix NADH (Shuttleworth, 2010). Seconds later, pyruvate oxidation is stimulated, leading to the mitochondrial NADH overshoot, likely compounded by the activation of ARALAR by cytosolic Ca^{2+} , which drives pyruvate into mitochondria and promotes respiration at moderate workloads (Lorente-Folch et al., 2013). By 10 s after the onset of stimulation, mitochondria are well energized with NADH, and perhaps also with ATP. Then, ATP is released to the cytosol through the ANT/VDAC under the fine control of the Na^+ pump, which is stimulated in a delayed fashion together with glycolysis.

Is ATP a physiological variable in neurons? The STB protocol represents a moderate degree of stimulation (Albensi et al., 2007) and did not affect ATP. Tetanic stimulation and glutamate further augmented the workload but failed to stimulate mitochondrial flux beyond that achieved by the STB, resulting in ATP depletion. Similar depletion has been reported in response to seizure-like activity or NMDA application (Toloe et al., 2014; Rueda et al., 2015; Lange et al., 2015; Rangaraju et al., 2014). It will be important to clarify whether ATP depletion occurs under strong physiological stimulation or whether it is a pathognomonic sign of neuronal dysfunction. According to computational modeling, a small decrease in cellular ATP may lead to runaway energy failure, a possible factor in the pathogenesis of neurodegeneration (Le Masson et al., 2014; Zilberter and Zilberter, 2017).

Limitations of Study

This work addressed neurons from hippocampus and somatosensory cortex of mice and it may not be representative of other types of neurons, or other species. Another caveat is that all measurements were on somata, which makes the metabolic behavior of distal dendrites and axons a matter of future enquiry.

STAR★METHODS

Detailed methods are provided in the online version of this paper and include the following:

- [KEY RESOURCES TABLE](#)
- [CONTACT FOR REAGENT AND RESOURCE SHARING](#)
- [EXPERIMENTAL MODEL AND SUBJECT DETAILS](#)
 - Mice
 - Embryonic Hippocampal Cultures
- [METHOD DETAILS](#)
 - Head Post, Chronic Window Implantation and Virus Injection
 - Immunofluorescence Staining
 - Fluorescent Measurements
 - Electrical Stimulation
 - Transport-stop and Pump-Inhibition Assays for Flux Measurements
 - Mathematical Modeling of ATP Homeostasis
 - Statistical Analysis

SUPPLEMENTAL INFORMATION

Supplemental Information includes seven figures and can be found with this article online at <https://doi.org/10.1016/j.cmet.2018.11.005>.

ACKNOWLEDGMENTS

We thank Karen Everett for critical reading of the manuscript, Francisco V. Sepúlveda for helpful comments, and Giovanni Marsicano, Bordeaux, for mito-GCaMP6s. This work was partly supported by FONDECYT grant 1160317 to L.F.B. B.W. is supported by the University of Zurich and the National Science Foundation and is a member of the Clinical Research Priority Program of the University of Zurich on Molecular Imaging. A.S.S. was supported by a long-term EMBO fellowship and a Synapsis Foundation career fellowship award. J.H. would like to thank Klaus-Armin Nave, Göttingen, for longstanding collaboration and ongoing support. The Centro de Estudios Científicos (CECs) is funded by the Chilean Government through the Centers of Excellence Basal Financing Program of CONICYT.

AUTHOR CONTRIBUTIONS

F.B.-L. conceived, designed and performed most of the *in vitro* experiments. R.G., V.L., E.D., M.H., M.V., and L.H. performed experiments. J.H. and J.S. contributed to the setting up of *in vivo* experiments. A.S.S. and B.W. conceived and designed experiments *in vivo* and prepared the respective figure. L.F.B. conceived and designed experiments *in vitro* and *in vivo*. F.B.-L. and L.F.B. analyzed data, prepared figures, and drafted the text. All authors discussed the data and critically revised the manuscript.

DECLARATION OF INTERESTS

Authors declare no competing interests.

Received: January 31, 2018

Revised: August 1, 2018

Accepted: November 12, 2018

Published: December 6, 2018

SUPPORTING CITATIONS

The following references appear in the Supplemental Information: [Ruminot et al., 2011](#), [Tantama and Yellen, 2014](#).

REFERENCES

- Albensi, B.C., Oliver, D.R., Toupin, J., and Otero, G. (2007). Electrical stimulation protocols for hippocampal synaptic plasticity and neuronal hyper-excitability: are they effective or relevant? *Exp. Neurol.* *204*, 1–13.
- Aubert, A., Pellerin, L., Magistretti, P.J., and Costalat, R. (2007). A coherent neurobiological framework for functional neuroimaging provided by a model integrating compartmentalized energy metabolism. *Proc. Natl. Acad. Sci. U S A* *104*, 4188–4193.
- Bak, L.K., and Walls, A.B. (2018). CrossTalk opposing view: lack of evidence supporting an astrocyte-to-neuron lactate shuttle coupling neuronal activity to glucose utilisation in the brain. *J. Physiol.* *596*, 351–353.
- Barres, B.A., Koroshetz, W.J., Chun, L.L., and Corey, D.P. (1990). Ion channel expression by white matter glia: the type-1 astrocyte. *Neuron* *5*, 527–544.
- Barros, L.F., and Martinez, C. (2007). An enquiry into metabolite domains. *Biophys. J.* *92*, 3878–3884.
- Barros, L.F., San Martin, A., Sotelo-Hitschfeld, T., Lerchundi, R., Fernández-Moncada, I., Ruminot, I., Gutiérrez, R., Valdebenito, R., Ceballos, S., Alegría, K., et al. (2013). Small is fast: astrocytic glucose and lactate metabolism at cellular resolution. *Front. Cell Neurosci.* *7*, 27.
- Barros, L.F., and Weber, B. (2018). CrossTalk proposal: an important astrocyte-to-neuron lactate shuttle couples neuronal activity to glucose utilisation in the brain. *J. Physiol.* *596*, 347–350.
- Berndt, N., Kann, O., and Holzhutter, H.G. (2015). Physiology-based kinetic modeling of neuronal energy metabolism unravels the molecular basis of NAD(P)H fluorescence transients. *J. Cereb. Blood Flow Metab.* *35*, 1494–1506.
- Bittner, C.X., Loaiza, A., Ruminot, I., Larenas, V., Sotelo-Hitschfeld, T., Gutiérrez, R., Córdova, A., Valdebenito, R., Frommer, W.B., and Barros, L.F. (2010). High resolution measurement of the glycolytic rate. *Front. Neuroenergetics* *2*, 1–11.
- Bittner, C.X., Valdebenito, R., Ruminot, I., Loaiza, A., Larenas, V., Sotelo-Hitschfeld, T., Moldenhauer, H., San Martín, A., Gutiérrez, R., Zambrano, M., and Barros, L.F. (2011). Fast and reversible stimulation of astrocytic glycolysis by K⁺ and a delayed and persistent effect of glutamate. *J. Neurosci.* *31*, 4709–4713.
- Blom, H., Ronnlund, D., Scott, L., Spicarova, Z., Widengren, J., Bondar, A., Aperia, A., and Brismar, H. (2011). Spatial distribution of Na⁺-K⁺-ATPase in dendritic spines dissected by nanoscale superresolution STED microscopy. *BMC Neurosci.* *12*, 16.
- Bouzier-Sore, A.K., Voisin, P., Bouchaud, V., Bezancon, E., Franconi, J.M., and Pellerin, L. (2006). Competition between glucose and lactate as oxidative energy substrates in both neurons and astrocytes: a comparative NMR study. *Eur. J. Neurosci.* *24*, 1687–1694.
- Brand, M.D., and Nicholls, D.G. (2011). Assessing mitochondrial dysfunction in cells. *Biochem. J.* *435*, 297–312.
- Chance, B., and Williams, G.R. (1956). The respiratory chain and oxidative phosphorylation. *Adv. Enzymol. Relat. Subj. Biochem.* *17*, 65–134.
- Connolly, N.M., Dussmann, H., Anilkumar, U., Huber, H.J., and Prehn, J.H. (2014). Single-cell imaging of bioenergetic responses to neuronal excitotoxicity and oxygen and glucose deprivation. *J. Neurosci.* *34*, 10192–10205.
- Deitch, J.S., and Banker, G.A. (1993). An electron microscopic analysis of hippocampal neurons developing in culture: early stages in the emergence of polarity. *J. Neurosci.* *13*, 4301–4315.
- Denton, R.M. (2009). Regulation of mitochondrial dehydrogenases by calcium ions. *Biochim. Biophys. Acta* *1787*, 1309–1316.
- Denton, R.M., Pullen, T.J., Armstrong, C.T., Heesom, K.J., and Rutter, G.A. (2016). Calcium-insensitive splice variants of mammalian E1 subunit of 2-oxoglutarate dehydrogenase complex with tissue-specific patterns of expression. *Biochem. J.* *473*, 1165–1178.
- Díaz-García, C.M., Mongeon, R., Lahmann, C., Koveal, D., Zucker, H., and Yellen, G. (2017). Neuronal stimulation triggers neuronal glycolysis and not lactate uptake. *Cell Metab.* *26*, 361–374.

- Diaz-Ruiz, R., Averet, N., Araiza, D., Pinson, B., Uribe-Carvajal, S., Devin, A., and Rigoulet, M. (2008). Mitochondrial oxidative phosphorylation is regulated by fructose 1,6-bisphosphate. A possible role in Crabtree effect induction? *J. Biol. Chem.* **283**, 26948–26955.
- Dobretsov, M., and Stimers, J.R. (2005). Neuronal function and alpha3 isoform of the Na/K-ATPase. *Front. Biosci.* **10**, 2373–2396.
- Du, F., Zhu, X.H., Zhang, Y., Friedman, M., Zhang, N., Ugurbil, K., and Chen, W. (2008). Tightly coupled brain activity and cerebral ATP metabolic rate. *Proc. Natl. Acad. Sci. U S A* **105**, 6409–6414.
- Duchen, M.R. (1992). Ca(2+)-dependent changes in the mitochondrial energetics in single dissociated mouse sensory neurons. *Biochem. J.* **283** (Pt 1), 41–50.
- Duchen, M.R., Verkhatsky, A., and Muallem, S. (2008). Mitochondria and calcium in health and disease. *Cell Calcium* **44**, 1–5.
- Erecinska, M., and Silver, I.A. (1994). Ions and energy in mammalian brain. *Prog. Neurobiol.* **43**, 37–71.
- Fein, A., and Tsacopoulos, M. (1988). Activation of mitochondrial oxidative metabolism by calcium ions in Limulus ventral photoreceptor. *Nature* **337**, 437–440.
- Fernandez-Moncada, I., and Barros, L.F. (2014). Non-preferential fuelling of the Na⁺/K⁺ ATPase pump. *Biochem. J.* **460**, 353–361.
- Gellerich, F.N., Gizatullina, Z., Gainutdinov, T., Muth, K., Seppet, E., Orynbayeva, Z., and Vielhaber, S. (2013). The control of brain mitochondrial energization by cytosolic calcium: the mitochondrial gas pedal. *IUBMB Life* **65**, 180–190.
- Genda, E.N., Jackson, J.G., Sheldon, A.L., Locke, S.F., Greco, T.M., O'Donnell, J.C., Spruce, L.A., Xiao, R., Guo, W., Putt, M., et al. (2011). Compartmentalization of the astroglial glutamate transporter, GLT-1, with glycolytic enzymes and mitochondria. *J. Neurosci.* **31**, 18275–18288.
- Glancy, B., and Balaban, R.S. (2012). Role of mitochondrial Ca²⁺ in the regulation of cellular energetics. *Biochemistry* **51**, 2959–2973.
- Hardie, D.G., Ross, F.A., and Hawley, S.A. (2012). AMPK: a nutrient and energy sensor that maintains energy homeostasis. *Nat. Rev. Mol. Cell Biol.* **13**, 251–262.
- Harris, J.J., Jolivet, R., and Attwell, D. (2012). Synaptic energy use and supply. *Neuron* **75**, 762–777.
- Hashimoto, T., Hussien, R., Cho, H.S., Kaufer, D., and Brooks, G.A. (2008). Evidence for the mitochondrial lactate oxidation complex in rat neurons: demonstration of an essential component of brain lactate shuttles. *PLoS One* **3**, e2915.
- Hauser, D.N., Mamais, A., Conti, M.M., Primiani, C.T., Kumaran, R., Dillman, A.A., Langston, R.G., Beilina, A., Garcia, J.H., Diaz-Ruiz, A., et al. (2017). Hexokinases link DJ-1 to the PINK1/parkin pathway. *Mol. Neurodegener.* **12**, 70.
- Heineman, F.W., and Balaban, R.S. (1990). Phosphorus-31 nuclear magnetic resonance analysis of transient changes of canine myocardial metabolism in vivo. *J. Clin. Invest.* **85**, 843–852.
- Herrero-Mendez, A., Almeida, A., Fernandez, E., Maestre, C., Moncada, S., and Bolanos, J.P. (2009). The bioenergetic and antioxidant status of neurons is controlled by continuous degradation of a key glycolytic enzyme by APC/C-Cdh1. *Nat. Cell Biol.* **11**, 747–752.
- Hertz, L., Drejer, J., and Schousboe, A. (1988). Energy metabolism in glutamatergic neurons, GABAergic neurons and astrocytes in primary cultures. *Neurochem. Res.* **13**, 605–610.
- Hill, A.V. (1950). A challenge to biochemists. *Biochim. Biophys. Acta* **4**, 4–11.
- Hochachka, P.W., and McClelland, G.B. (1997). Cellular metabolic homeostasis during large-scale change in ATP turnover rates in muscles. *J. Exp. Biol.* **200**, 381–386.
- Imamura, H., Nhat, K.P., Togawa, H., Saito, K., Iino, R., Kato-Yamada, Y., Nagai, T., and Noji, H. (2009). Visualization of ATP levels inside single living cells with fluorescence resonance energy transfer-based genetically encoded indicators. *Proc. Natl. Acad. Sci. U S A* **106**, 15651–15656.
- Jekabsons, M.B., and Nicholls, D.G. (2004). In situ respiration and bioenergetic status of mitochondria in primary cerebellar granule neuronal cultures exposed continuously to glutamate. *J. Biol. Chem.* **279**, 32989–33000.
- Jolivet, R., Coggan, J.S., Allaman, I., and Magistretti, P.J. (2015). Multi-time-scale modeling of activity-dependent metabolic coupling in the neuron-glia-vasculature ensemble. *PLoS Comput. Biol.* **11**, e1004036.
- Juhaszova, M., and Blaustein, M.P. (1997). Na⁺ pump low and high ouabain affinity alpha subunit isoforms are differently distributed in cells. *Proc. Natl. Acad. Sci. U S A* **94**, 1800–1805.
- Lamy, C.M., and Chatton, J.Y. (2011). Optical probing of sodium dynamics in neurons and astrocytes. *Neuroimage* **58**, 572–578.
- Lange, S.C., Winkler, U., Andresen, L., Byhro, M., Waagepetersen, H.S., Hirrlinger, J., and Bak, L.K. (2015). Dynamic changes in cytosolic ATP levels in cultured glutamatergic neurons during NMDA-induced synaptic activity supported by glucose or lactate. *Neurochem. Res.* **40**, 2517–2526.
- Le Masson, G., Przedborski, S., and Abbott, L.F. (2014). A computational model of motor neuron degeneration. *Neuron* **83**, 975–988.
- Li, H., Wang, X., Zhang, N., Gottipati, M.K., Parpura, V., and Ding, S. (2014). Imaging of mitochondrial Ca²⁺ dynamics in astrocytes using cell-specific mitochondria-targeted GCaMP5G/6s: mitochondrial Ca²⁺ uptake and cytosolic Ca²⁺ availability via the endoplasmic reticulum store. *Cell Calcium* **56**, 457–466.
- Llorente-Folch, I., Rueda, C.B., Amigo, I., del, A.A., Saheki, T., Pardo, B., and Satrustegui, J. (2013). Calcium-regulation of mitochondrial respiration maintains ATP homeostasis and requires ARALAR/AGC1-malate aspartate shuttle in intact cortical neurons. *J. Neurosci.* **33**, 13957–13971, 13971a.
- Machler, P., Wyss, M.T., Elsayed, M., Stobart, J., Gutierrez, R., von Faber-Castell, A., Kaelin, V., Zuend, M., San, M.A., Romero-Gomez, I., et al. (2016). In vivo evidence for a lactate gradient from astrocytes to neurons. *Cell Metab.* **23**, 94–102.
- Mamczur, P., Borsuk, B., Paszko, J., Sas, Z., Mozrzymas, J., Wisniewski, J.R., Gizak, A., and Rakus, D. (2015). Astrocyte-neuron crosstalk regulates the expression and subcellular localization of carbohydrate metabolism enzymes. *Glia* **63**, 328–340.
- Mayrhofer, J.M., Haiss, F., Haenni, D., Weber, S., Zuend, M., Barrett, M.J., Ferrari, K.D., Maechler, P., Saab, A.S., Stobart, J.L., et al. (2015). Design and performance of an ultra-flexible two-photon microscope for in vivo research. *Biomed. Opt. Express* **6**, 4228–4237.
- Morris, C.E., Wang, J.A., and Markin, V.S. (2003). The invagination of excess surface area by shrinking neurons. *Biophys. J.* **85**, 223–235.
- Ohkura, M., Sasaki, T., Sadakari, J., Gengyo-Ando, K., Kagawa-Nagamura, Y., Kobayashi, C., Ikegaya, Y., and Nakai, J. (2012). Genetically encoded green fluorescent Ca²⁺ indicators with improved detectability for neuronal Ca²⁺ signals. *PLoS One* **7**, e51286.
- Pandya, J.D., Nukala, V.N., and Sullivan, P.G. (2013). Concentration dependent effect of calcium on brain mitochondrial bioenergetics and oxidative stress parameters. *Front. Neuroenergetics* **5**, 10.
- Pellerin, L., and Magistretti, P.J. (1994). Glutamate uptake into astrocytes stimulates aerobic glycolysis: a mechanism coupling neuronal activity to glucose utilization. *Proc. Natl. Acad. Sci. U S A* **91**, 10625–10629.
- Pellerin, L., and Magistretti, P.J. (1997). Glutamate uptake stimulates Na⁺, K⁺-ATPase activity in astrocytes via activation of a distinct subunit highly sensitive to ouabain. *J. Neurochem.* **69**, 2132–2137.
- Pologruto, T.A., Sabatini, B.L., and Svoboda, K. (2003). ScanImage: flexible software for operating laser scanning microscopes. *Biomed. Eng. Online* **2**, 13.
- Porras, O.H., Loaiza, A., and Barros, L.F. (2004). Glutamate mediates acute glucose transport inhibition in hippocampal neurons. *J. Neurosci.* **24**, 9669–9673.
- Rangaraju, V., Calloway, N., and Ryan, T.A. (2014). Activity-driven local ATP synthesis is required for synaptic function. *Cell* **156**, 825–835.
- Rose, C.R., and Ransom, B.R. (1997). Regulation of intracellular sodium in cultured rat hippocampal neurones. *J. Physiol.* **499** (Pt 3), 573–587.

- Rose, E.M., Koo, J.C., Antflick, J.E., Ahmed, S.M., Angers, S., and Hampson, D.R. (2009). Glutamate transporter coupling to Na,K-ATPase. *J. Neurosci.* *29*, 8143–8155.
- Rueda, C.B., Traba, J., Amigo, I., Llorente-Folch, I., Gonzalez-Sanchez, P., Pardo, B., Esteban, J.A., del, A.A., and Satrustegui, J. (2015). Mitochondrial ATP-Mg/Pi carrier SCaMC-3/Slc25a23 counteracts PARP-1-dependent fall in mitochondrial ATP caused by excitotoxic insults in neurons. *J. Neurosci.* *35*, 3566–3581.
- Ruminot, I., Gutiérrez, R., Peña-Munzenmeyer, G., Añazco, C., Sotelo-Hitschfeld, T., Lerchundi, R., Niemeyer, M.I., Shull, G.E., and Barros, L.F. (2011). NBCE1 mediates the acute stimulation of astrocytic glycolysis by extracellular K⁺. *J. Neurosci.* *31*, 14264–14271.
- Saks, V., Beraud, N., and Wallimann, T. (2008). Metabolic compartmentation - a system level property of muscle cells: real problems of diffusion in living cells. *Int. J. Mol. Sci.* *9*, 751–767.
- San Martín, A., Ceballos, S., Baeza-Lehnert, F., Lerchundi, R., Valdebenito, R., Contreras-Baeza, Y., Alegria, K., and Barros, L.F. (2014). Imaging mitochondrial flux in single cells with a FRET sensor for pyruvate. *PLoS One* *9*, e85780.
- San Martín, A., Ceballos, S., Ruminot, I., Lerchundi, R., Frommer, W.B., and Barros, L.F. (2013). A genetically encoded FRET lactate sensor and its use to detect the Warburg effect in single cancer cells. *PLoS One* *8*, e57712.
- Shuttleworth, C.W. (2010). Use of NAD(P)H and flavoprotein autofluorescence transients to probe neuron and astrocyte responses to synaptic activation. *Neurochem. Int.* *56*, 379–386.
- Takanaga, H., Chaudhuri, B., and Frommer, W.B. (2008). GLUT1 and GLUT9 as major contributors to glucose influx in HepG2 cells identified by a high sensitivity intramolecular FRET glucose sensor. *Biochim. Biophys. Acta* *1778*, 1091–1099.
- Tantama, M., Martinez-Francois, J.R., Mongeon, R., and Yellen, G. (2013). Imaging energy status in live cells with a fluorescent biosensor of the intracellular ATP-to-ADP ratio. *Nat. Commun.* *4*, 2550.
- Tantama, M., and Yellen, G. (2014). Imaging changes in the cytosolic ATP-to-ADP ratio. *Methods Enzymol.* *547*, 355–371.
- Tarasov, A.I., Semplici, F., Ravier, M.A., Bellomo, E.A., Pullen, T.J., Gilon, P., Sekler, I., Rizzuto, R., and Rutter, G.A. (2012). The mitochondrial Ca²⁺ uniporter MCU is essential for glucose-induced ATP increases in pancreatic beta-cells. *PLoS One* *7*, e39722.
- Tescarollo, F., Covolani, L., and Pellerin, L. (2014). Glutamate reduces glucose utilization while concomitantly enhancing AQP9 and MCT2 expression in cultured rat hippocampal neurons. *Front. Neurosci.* *8*, 246.
- Toloe, J., Mollajew, R., Kugler, S., and Mironov, S.L. (2014). Metabolic differences in hippocampal 'Rett' neurons revealed by ATP imaging. *Mol. Cell Neurosci.* *59*, 47–56.
- Trevisiol, A., Saab, A.S., Winkler, U., Marx, G., Imamura, H., Mobius, W., Kusch, K., Nave, K.A., and Hirrlinger, J. (2017). Monitoring ATP dynamics in electrically active white matter tracts. *Elife* *6*, <https://doi.org/10.7554/eLife.24241>.
- Westermann, B. (2015). The mitochondria-plasma membrane contact site. *Curr. Opin. Cell Biol.* *35*, 1–6.
- Wilson, D.F. (2017). Oxidative phosphorylation: regulation and role in cellular and tissue metabolism. *J. Physiol.* *595*, 7023–7038.
- Wyss, M.T., Jolivet, R., Buck, A., Magistretti, P.J., and Weber, B. (2011). In vivo evidence for lactate as a neuronal energy source. *J. Neurosci.* *31*, 7477–7485.
- Zilberter, Y., and Zilberter, M. (2017). The vicious circle of hypometabolism in neurodegenerative diseases: ways and mechanisms of metabolic correction. *J. Neurosci. Res.* *95*, 2217–2235.

STAR★METHODS

KEY RESOURCES TABLE

REAGENT or RESOURCE	SOURCE	IDENTIFIER
Antibodies		
Mouse monoclonal anti-NeuN (clone A60)	Millipore	Cat. #MAB377; RRID:AB_2298772
Rabbit polyclonal anti-Glial fibrillary acidic protein	Dako	Cat. #Z0334; RRID:AB_10013382
Anti-mouse Alexa Fluor 488	Jackson	Cat. #715-546-150; RRID:AB_2340849
Anti-rabbit DyLight-549	Jackson	Cat. #111-506-003
Bacterial and Virus Strains		
AAV9-hSyn-RCaMP1.07	Custom preparation at University of Zurich and UNC Viral Core Facility	N/A
Chemicals, Peptides, and Recombinant Proteins		
Cytochalasin B	Millipore	CAS: 14930-96-2
AR-C 155858	Haoyuan Chemexpress	CAS: 496791-37-8
Ouabain octahydrate	Sigma-Aldrich	CAS: 11018-89-6
(+)-MK 801 maleate	Tocris	CAS: 77086-22-7
DNQX	Tocris	CAS: 2379-57-9
TTX	Sigma-Aldrich	CAS: 4368-28-9
BCECF,AM (2',7'-Bis-(2-Carboxyethyl)-5-(and-6)-Carboxyfluorescein, Acetoxymethyl Ester)	Invitrogen	Cat. #B1170
Fluo 4, AM, cell permeant	Invitrogen	Cat. #F14201
Rhod-2, AM, cell permeant	Invitrogen	Cat. #R1245MP
SBFI, AM	TEFlabs	Cat. #0031
Asante Natrium Green	TEFlabs	Cat. # 3512
Critical Commercial Assays		
Lipofectamine 3000 Transfection Reagent	Invitrogen	Cat. #L3000015
Experimental Models: Organisms/Strains		
Mouse:C57BL/6J x CBA/J	The Jackson Laboratory	JAX: 100011
Mouse:B6-Tg(Thy1.2-ATeam1.03 ^{YEMK_AJhi})	Trevisiol et al., 2017	N/A
Recombinant DNA		
Plasmid: FLII12Pglu700 μ Δ 6	Takanaga et al., 2008	Addgene plasmid #17866
Plasmid: Pyronic	San Martin et al., 2014	Addgene plasmid #51308
Plasmid: Laconic	San Martin et al., 2013	Addgene plasmid #44238
Plasmid: ATeam 1.03	Imamura et al., 2009	Addgene plasmid #51958
Plasmid: RCaMP1.07	Ohkura et al., 2012	N/A
Plasmid: Perceval HR	Tantama et al., 2013	Addgene plasmid #49082
Plasmid: mito-GCaMP6s	Lamy and Chatton, 2011	N/A
Software and Algorithms		
Berkeley Madonna 8.3.23.0	University of California at Berkeley	http://www.berkeleymadonna.com
Fluoview FV10-ASW 3.0	Olympus	N/A
Metafluor 7.5.0.0	Molecular Devices	https://www.moleculardevices.com/systems/metamorph-research-imaging/metafluor-fluorescence-ratio-imaging-software
Kinetics 6.0.2.40	Kinetic imaging	N/A
ImageJ 1.49m	NIH	http://imagej.net

CONTACT FOR REAGENT AND RESOURCE SHARING

Further information and requests for resources and reagents should be directed to the Lead Contact, L. Felipe Barros (fbarros@cecs.cj).

EXPERIMENTAL MODEL AND SUBJECT DETAILS

Mice

For *in vivo* experiments, animals used were mixed F1 2-6 month-old female and male mice (C57BL/6J x CBA/J), which were kept in under SPF conditions at room temperature ($20 \pm 2^\circ\text{C}$) in a 12/12 h light/dark cycle with free access to food and water. *In vivo* 2-photon imaging in transgenic ATP sensor mice (B6-Tg(Thy1.2-Ateam1.03^{YEMK})^{AJhi}) (Trevisiol et al., 2017) were approved by the local veterinary authorities in Zurich and conformed to the guidelines of the Swiss Animal Protection Law, Veterinary Office, Canton of Zurich (Act of Animal Protection 16 December 2005 and Animal Protection Ordinance 23 April 2008). Surgery was performed in female mice of 10-12 weeks of age (20–25 g bodyweight). Mice were housed in groups of 2-4, had free access to food and water and were kept under an inverted 12 hour light/dark cycle. For *in vitro* experiments, animals used were 17.5 days-old embryos of mixed sex (C57BL/6J x CBA/J). Pregnant female mice were kept in under SPF conditions at room temperature ($20 \pm 2^\circ\text{C}$) in a 12/12 h light/dark cycle with free access to food and water. Experiments were approved by the Centro de Estudios Científicos Animal Care and Use Committee.

Embryonic Hippocampal Cultures

Pregnant mice were sacrificed by cervical dislocation and 6-8 embryos were transferred to ice-cold HBSS medium supplemented with 5mM glucose. The brains were extracted and the hippocampus was dissected free of meninges. The tissue was enzymatically dissociated in HBSS containing 1% trypsin-EDTA (Sigma-Aldrich) for 15 minutes at 37°C and then the digestion was stopped by addition of Neurobasal medium (Gibco) containing 10mM glucose, 2% B-27 supplement, 1% glutamax and 5% FBS. After mechanical dissociation, cells were plated in poly-D-lysine-coated glass coverslips for three hours, followed by removal of medium and addition of 2ml of serum-free Neurobasal Medium (Gibco) containing 10 mM glucose, 2% B-27 supplement, 1% glutamax, 2.5 $\mu\text{g/ml}$ fungizone and 10 $\mu\text{g/ml}$ penicillin/streptomycin. Cultures were kept at 37°C in a humid atmosphere (95% air/ 5% CO_2) and 2/3 of the medium was replaced every three days. Cells were transfected at days 10-12 with Lipofectamine 3000 (Invitrogen) using 3 μg of sensor plasmid DNA, 6 μg of lipofectamine reagent and 3 μg of P300 reagent. Experiments were performed at days 11-15. To test for their effect on neuronal glucose dynamics (Figure S1), 8-10 day old mouse cortical astrocytes (Bittner et al., 2010) from a single 35 mm dish were trypsinized, washed 3 times in 10% serum medium for trypsin inactivation, and seeded on three 35 mm dishes with neurons, 24 hours before fluorescence measurements.

METHOD DETAILS

Head Post, Chronic Window Implantation and Virus Injection

Head post and chronic window implantation were performed as previously described (Machler et al., 2016). Head post implantation was conducted under isoflurane anesthesia (4% for induction, 1-2% for maintenance). Animals were fixed in a stereotaxic frame and following a midline incision the skull was exposed. After careful cleaning of the bone, several layers of light-cured dental cement (Tetric EvoFlow) were used to attach an aluminum head post to the back of the head. The skull over the left somatosensory cortex was left exposed for craniotomy. Two days after head post implantation a craniotomy was cut over the primary sensory cortex under midazolam (5 mg/kg), fentanyl (0.05 mg/kg) and medetomidine (0.5 mg/kg) anesthesia. Intrinsic optical imaging was used to map the somatosensory regions for proper localization before craniotomy. 150 – 200 nl of virus vector AAV9-hSYN-RCaMP1.07 (titer 2.4 E12 VG/ml) was injected with a pipette and a hydraulic pump into the hindpaw and/or whisker barrel areas at a depth of 350 – 400 nm. Following virus injection a 3 x 3 mm square coverslip was gently placed over the exposed brain and fixed with dental cement to the head cap. Mice were allowed to recover for at least 3 weeks before *in vivo* imaging experiments.

Immunofluorescence Staining

Cultures were fixed for 30 min in 2% paraformaldehyde at 4°C , washed 3 times with 2ml of PBS, and permeabilized with 3% Triton X100 in PBS containing 2% normal goat serum. Cells were incubated overnight at 4°C with mouse anti-NeuN (0.1 $\mu\text{g/ml}$; Millipore) and rabbit anti-GFAP (4 $\mu\text{g/ml}$; DAKO) antisera. Secondary antibodies were Alexa-488 and DyLight-549, both from Jackson. Images were captured using an Olympus FV1000 fluorescence microscope.

Fluorescent Measurements

Primary Culture Imaging

Cells were imaged at room temperature ($22 - 25^\circ\text{C}$) in a 95% air/5% CO_2 -gassed solution of the following composition (in mM): 112 NaCl, 3 KCl, 1.25 CaCl_2 , 1.25 MgSO_4 , 1-2 glucose, 1 lactate, 10 HEPES, 24 NaHCO_3 , pH 7.4, using an upright Olympus FV1000 Confocal Microscope equipped with a water immersion objectives (10x, NA 0.3; 20x, NA 0.95) and 440, 488 and 543 nm lasers. Alternatively, cells were imaged with an Olympus IX70 or with an Olympus BX51 microscope equipped with a 40x oil-immersion

objective (NA 1.3) or with a 20x water immersion objective (NA 1.0). Bright field microscopes were equipped with CAIRN monochromators (Faversham, UK), and either a Hamamatsu Orca camera controlled by Kinetics software or a Rollera camera controlled with MetaFluor software, respectively. FRET sensors (FLII12Pglu700 $\mu\Delta$ 6, Laconic, Pyronic and ATeam) were excited at 440 nm (Confocal) or 430 nm (monochromator). Perceval HR and BCECF were excited at 430 and 490 nm (monochromator). Mito-GCaMP6s, Fluo4, Asante Natrium Green and Calcein were excited at 488 nm (Confocal) or 490 nm (monochromator). Rhod2 and Calcein Orange were excited at 543 nm. The effect of pH on Perceval HR (Tantama et al., 2013) during OXPHOS inhibition was corrected as explained in Figure S5. FRET data are presented as the ratio between CFP or mTFP emission and YFP or Venus emission respectively, normalized with respect to the minimum ratio obtained in the absence of glucose for the FLII12Pglu700 $\mu\Delta$ 6 sensor, and the initial steady state kept by a reference buffer containing 2mM glucose and 1mM lactate for Pyronic, Laconic, ATeam and Perceval HR sensors. Full calibration of FLII12Pglu700 $\mu\Delta$ 6 in neurons is not practical because they express the high affinity transporter GLUT3, which slows down glucose equilibration at high concentrations. Figure S4 shows that the change of FRET ratio of the sensor expressed in neurons is similar to that previously described *in vitro* (Takanaga et al., 2008) and in several other cell types (Bittner et al., 2010).

AM dyes were loaded in 0.02% pluronic acid. Fluo4, Calcein and Calcein Orange were ester loaded at 4 μ M in culture medium for 30 minutes. Asante Natrium Green was ester loaded under the same conditions for 1 hour. SBFI was ester loaded at 20 μ M for 1 hour. BCECF was ester loaded at 2 μ M at room temperature for 5 minutes. Rhod-2 was ester loaded at 4 μ M at 4°C for 15 minutes in HEPES buffer supplemented with glucose and lactate, and then incubated overnight in culture medium before experiments. Calibration of SBFI and Asante Natrium Green was done at the end of each experiment in the presence of gramicidine, nigericine and ouabain, as described by Rose and Ransom (1997). At the time indicated, the Na⁺ concentration of the recording solution was reduced to 80 mM (referred to as Low Na⁺) and the osmolarity was compensated with N-methyl-D-glucamine.

In vivo Imaging

In vivo imaging of cortical neurons (layers 2/3, 150–200 μ m below the dura) was carried out in transgenic mice B6-Tg(Thy1.2-ATeam1.03^{YEMK_AJhi}), which express ATeam specifically in neurons (Trevisiol et al., 2017). Anesthesia, head-post implantation, craniotomy and virus injection have been performed as described previously (Machler et al., 2016). In order to monitor neuronal calcium changes in addition to cytosolic ATP dynamics, we injected 150–200 nl of virus vector AAV9-hSYN-RCaMP1.07 (titer 2.4 E12 VG/ml) into the somatosensory cortex. Following robust RCaMP1.07 sensor expression calcium and ATP imaging started around 3 weeks after virus injection. Mice were imaged using a custom-built two-photon laser scanning microscope (2PLSM; (Mayrhofer et al., 2015) with a tunable pulsed laser (MaiTai eHP DS system or InSightTM DeepSee system, Spectra-Physics) at 870 and 1100 nm wavelength (for ATP sensor and calcium sensor imaging, respectively) equipped with a 20x water immersion objective (W-Plan-Apochromat 20x/1.0 Differential Interference Contrast, Zeiss). During measurements, animals were head-fixed and kept under isoflurane (1.5 %) anesthesia. Unidirectional frame scans at 11.84 or 1.53 Hz and 128 x 128 or 512 x 512 pixel resolution, respectively, were acquired with ScanImage (r3.8.1, Janelia Research Campus; Pologruto et al., 2003). The following Semrock bandpass filters were used 475/64, 542/50 and 607/70, to detect emission of the FRET pair mseCFP and cp173-mVenus as well as emission of RCaMP1.07. For ATP FRET analysis the Venus channel was divided by the CFP channel and the ratio normalized to the corresponding baseline. Images were processed using ImageJ software (1.49m; NIH, USA) and mainly on whole frames. For neuronal calcium RCaMP1.07 emission analysis, time acquisition curves were normalized to initial frames to monitor relative changes in calcium transients. ATP channel acquisitions and calcium imaging of the same neurons were performed sequentially by changing excitation wavelengths accordingly. Three to five mice, each having up to 3 different regions of interest (containing 6–15 neurons), were analyzed for spontaneous, sensory-evoked activities and cortical microstimulations.

Electrical Stimulation

Field Stimulation

Mixed cultures of hippocampal neurons and astrocytes grown on 25 mm coverslips were field-stimulated using a RC-21BRFS chamber (Warner Instruments) and a PRO-4 device (World Precision Instruments, WPI). Pulses (50mA output) were generated with a WPI A385 High Current Stimulus Isolator connected to a WPI A382 Battery Charger. The stimulation protocol was a short theta burst that mimics hippocampal activity, consisting of two trains of impulses separated by 10 seconds. Each train lasted for 1 second and was composed of twenty pulses of 1 ms duration, distributed into five groups of four pulses (illustrated in Figure 1A). Alternatively, cultures were subjected to tetanic stimulation (20 Hz for 30s).

Mice Stimulation

In vivo cortical neuronal activity was evoked either by sensory stimulation (whisker-pad or hind-limb) or by micro-stimulation with a glass electrode inserted into cortical layers 2 to 3. Whisker-pad and hind-limb were stimulated with 400 μ A either at 2 or 4 Hz for various durations of 2, 4, 8 and 10 s or for 1 min and the corresponding cortical area was imaged. For intracortical microstimulations a 16x water-immersion objective (LWD 16x/0.80 DIC N2, Nikon) was used. Glass capillaries (Science Products; GB120F-8P 0.69 x 1.20 x 80 mm with filament) were pulled to achieve an impedance of 1.5 M Ω at 1 kHz, backfilled with Artificial Cerebrospinal Fluid, ACSF (containing in mM: 140 NaCl, 4 KCl, 2 CaCl₂, 2 MgCl₂, 10 glucose and 10 HEPES) and inserted below the remaining cranial glass window into the cortex. The glass of the cranial window was partly removed after carefully splitting it with a diamond glass cutter. Local stimulation was applied with a square-wave constant current stimulus (ranging from 5 to 50 μ A) for 1 min (1 Hz train frequency, 100 ms trains at 330 or 100 Hz) using a constant-current isolator (STG 4002, Multi Channel Systems).

Transport-stop and Pump-Inhibition Assays for Flux Measurements

Fluxes were measured using genetically-encoded FRET sensors by acute pharmacological interruption of metabolite steady states with transport blockers as reported (Bittner et al., 2010; Barros et al., 2013). Glucose consumption rate was computed in the presence of the GLUT blocker cytochalasin B (20 μM) before (3 min) and after STB stimulation. Mitochondrial pyruvate consumption was measured in the presence of the MCT blocker AR-C155858 (1 μM) before (3 min) and after STB stimulation. Lactate depletion/accumulation was detected by exposure to 1 μM AR-C155858. Linear regressions were used to estimate fluxes. The onset of flux stimulation was computed as the intersection between linear regressions before and after STB. The effect of Na^+ pump inhibition over ATP and the ADP:ATP ratio was estimated by exposing cells to either 0.1mM ouabain or a potassium-free buffer before (1 min) and after STB stimulation.

Mathematical Modeling of ATP Homeostasis

The predicted response of neuronal energy status to electrical stimulation (STB) and Na^+ pump inhibition under a homeostatic control system was determined by numerical simulation using Berkeley Madonna software. Metabolite pools were modeled according to (Aubert et al., 2007; Jolivet et al., 2015) and the following equations:

$$d\text{ATP}/dt = \text{Prod} - (\text{pump} + \text{housekeeping}) + K_{\text{off}} * \text{PCr} * \text{ADP} - K_{\text{on}} * \text{ATP} * \text{Cr}$$

$$\text{ADP} = \text{ATP}/2 * (-ak + (ak^2 + 4 * ak * (A/\text{ATP} - 1))^{1/2})$$

$$\text{AMP} = A - (\text{ATP} + \text{ADP})$$

$$d\text{Cr}/dt = K_{\text{off}} * \text{PCr} * \text{ADP} - K_{\text{on}} * \text{ATP} * \text{Cr}$$

$$d\text{PCr}/dt = K_{\text{on}} * \text{ATP} * \text{Cr} - K_{\text{off}} * \text{PCr} * \text{ADP}$$

where *prod* is the sum of glycolytic and mitochondrial ATP production, *pump* is the ATP consumption of the Na^+/K^+ ATPase, *housekeeping* is the ATP consumption of other processes, K_{on} and K_{off} are the kinetic constants of creatine kinase, *PCr* is phosphocreatine, *Cr* is creatine, *ak* is adenylate kinase, and *A* is the full nucleotide pool ($\text{ATP} + \text{ADP} + \text{AMP}$). *A* was set at 1.554 mM and *ak* at 1 to obtain a resting ATP of 1.4 mM (Rangaraju et al., 2014). *Prod* was set at $0.53 * \text{ADP} / (1.26 + \text{ADP})$ to obtain a sensitive negative feedback in which resting ATP production is 10% of maximum ATP production. Alternatively, *Prod* was set at $0.053 + 0.001 * (1.4 - \text{ATP}) + 0.001 * (\text{ADP} - 0.14)$ (Le Masson et al., 2014; Figure S5). To simulate ultrasensitivity while setting ATP production at 10% of maximum ATP production using the equation $\text{Prod} = 0.53 * \text{ADP}^H / (K_M^H + \text{ADP}^H)$, the respective values of the Hill coefficient and the affinity constant (*H*, *K_M*) where (1, 1.26; 2, 0.42; 4, 0.2425; 10, 0.17441; 100, 0.1431103). Resting ATP production (53 $\mu\text{M}/\text{s}$) was inferred from the resting glucose plus lactate consumption of 1.7 $\mu\text{M}/\text{s}$ glucose equivalents (Figure S4B) and 31 ATPs generated per each glucose equivalent. Resting *PCr* and *Cr* were respectively set at 2.7 and 0.09 mM (Hertz et al., 1988; Jolivet et al., 2015). $K_{\text{on}} = 3.9 \text{ mM}^{-1} * \text{s}^{-1}$ and $K_{\text{off}} = 1.3 \text{ mM}^{-1} * \text{s}^{-1}$ were set at high values to maximize the buffering effect of creatine kinase. ATeam and Perceval HR signals were simulated according to their saturation parameters:

$$\text{ATeam} = 1 + 1.3 * \text{ATP}^{2.1} / (3.3^{2.1} + \text{ATP}^{2.1}); \text{ (Imamura et al., 2009).}$$

$$\text{Perceval HR} = 1 + 2.5 * \text{ratio}^{0.97} / (3.5^{0.97} + \text{ratio}^{0.97}); \text{ (Tantama et al., 2013).}$$

Statistical Analysis

Statistical analyses were carried out with SigmaPlot software (Jandel). For normally distributed variables, differences were assessed with the Student's *t*-test (pairs) and with ANOVA followed by the Tukey-Kramer *ad hoc* test (groups). For variables that failed the normality test, differences were assessed with the Mann-Whitney-Wilcoxon signed rank test (pairs) or with the Kruskal-Wallis one way ANOVA on ranks (groups). *, $p < 0.05$; ns (non-significant), $p > 0.05$. The number of experiments and cells is detailed in each figure.